

# **The Critical Role of Volatile Organic Compounds Emission in Nitrate Formation in Lhasa, Tibetan Plateau: Insights from Oxygen Isotope Anomaly Measurements**

Xueqin Zheng<sup>a</sup>, Junwen Liu<sup>a\*</sup>, Nima Chuduo<sup>b</sup>, Bian Ba<sup>b</sup>, Pengfei Yu<sup>a</sup>, Phu Drolgar<sup>b</sup>, Fang Cao<sup>c</sup>,  
Yanlin Zhang<sup>c</sup>

<sup>a</sup> College of Environment and Climate, Jinan University, Guangzhou, 511443, China

<sup>b</sup> Lhasa Meteorological Administration, Lhasa, 850010, China

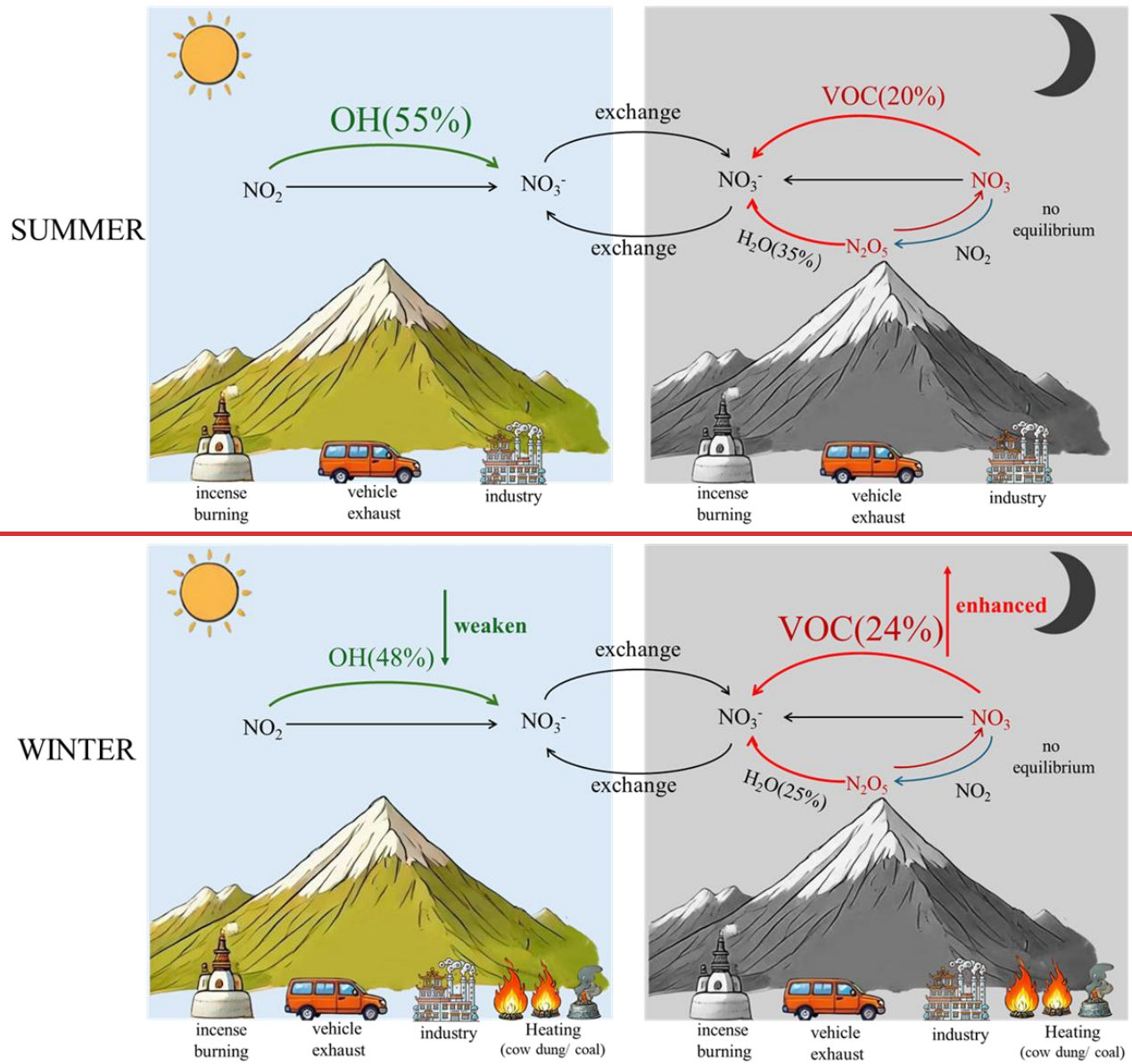
<sup>c</sup> School of Ecology and Applied Meteorology, Nanjing University of Information Science and Technology, Nanjing 210044, China

\* Corresponding author: [Junwen Liu](#)

[email: liu.junwen@jnu.edu.cn](mailto:liu.junwen@jnu.edu.cn)

27

28



29

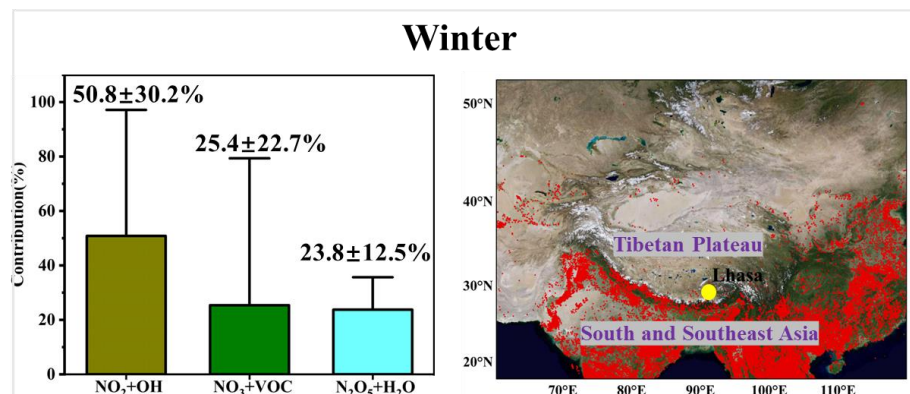
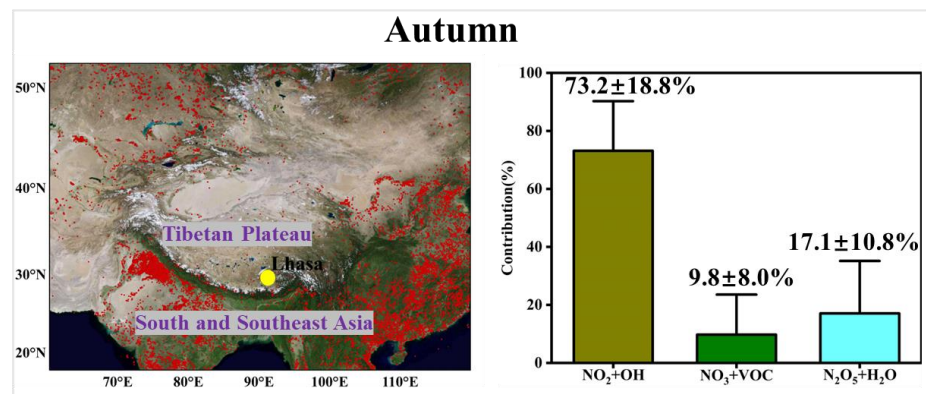
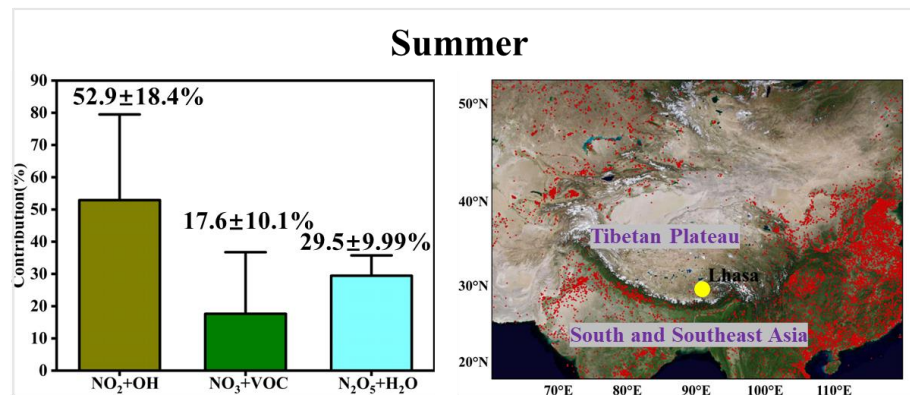
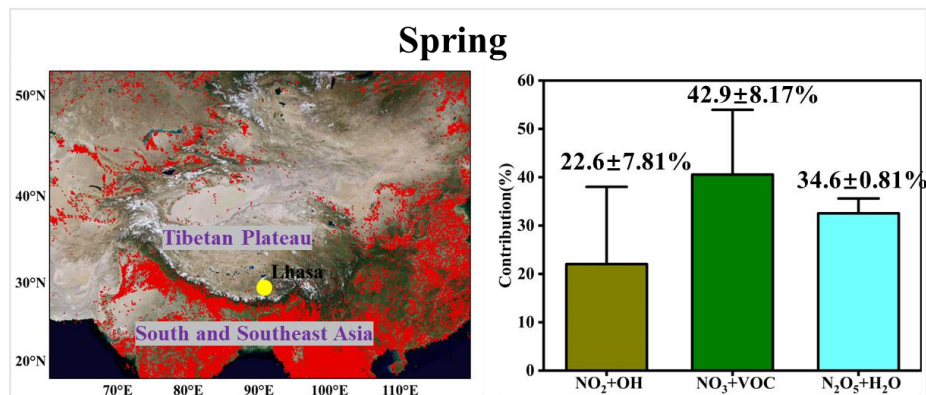
30

31

32

33

34



## Abstract

Atmospheric particulate nitrate aerosol ( $\text{NO}_3^-$ ), produced via the oxidation of nitrogen oxides ( $\text{NO}_x = \text{NO} + \text{NO}_2$ ), plays an important role in atmospheric chemistry and air quality, yet its formation mechanism ~~remains still~~ poorly constrained in the plateau region. In this study, we ~~first~~ reported for the first time the yearly variation ~~of in~~ the signatures ~~for of~~ the stable oxygen isotope anomaly ( $\Delta^{17}\text{O} = \delta^{17}\text{O} - 0.52 \times \delta^{18}\text{O}$ ) in  $\text{NO}_3^-$  collected in the urban ~~region of Lhasa city~~ Lhasa (3650 m a.s.l), on the Tibetan Plateau, China. Our results show that  $\text{NO}_2 + \text{OH}$  ~~is was~~ the largest contributor to  $\text{NO}_3^-$  formation ( $46 \pm 26\%$ ), followed by  $\text{NO}_3 + \text{VOC}$  ( $26 \pm 18\%$ ), and  $\text{N}_2\text{O}_5 + \text{H}_2\text{O}$  ( $28 \pm 11\%$ ) using the Bayesian Isotope Mixture Model. Notably, there ~~are were~~ significant differences in the  $\text{NO}_2 + \text{OH}$ ,  $\text{NO}_3 + \text{VOC}$ , and  $\text{N}_2\text{O}_5 + \text{H}_2\text{O}$  pathways between spring and the other three seasons (T test,  $p < 0.05$ ). By Hybrid Single-Particle Lagrangian Integrated Trajectory (HYSPPLIT) dispersion model, we ~~Our results~~ highlighted the influence of VOC emissions from regions such as Afghanistan and northern India, which enhanced NO $_3^-$  concentrations in Lhasa during spring. Furthermore, the diurnal distribution of  $\text{NO}_3^-$  oxidation pathways varied distinctly across seasons, suggesting that these differences in  $\text{NO}_3^-$  pathways are attributed to aerosol liquid water content (ALWC), volatile organic compounds (VOC) concentrations, and ~~pollution level~~ atmospheric lifetime of  $\text{NO}_3^-$ s.

**Keywords:** nitrate,  $\Delta^{17}\text{O}$ - $\text{NO}_3^-$ , oxidation pathways, Lhasa, VOC

## 1. Introduction

Nitrate aerosol ( $\text{NO}_3^-$ ) is a key component regulating the mass concentration of atmospheric fine particulate matter ( $\text{PM}_{2.5}$ ), which is highly related with air quality (Colmer et al., 2020), public health (Zhang et al., 2019; Zhang et al., 2017; Geng et al., 2021), and climate system (Clark and Tilman, 2008). Globally, the mass contribution of  $\text{NO}_3^-$  in  $\text{PM}_{2.5}$  is in the range of 5-30% (Huang et al., 2014; Xu et al., 2019; Salameh et al., 2015; Espina-Martin et al., 2024; Bell et al., 2007; Sun et al., 2022), depending on the locations and the severities of air pollution. For example, it was reported that  $\text{NO}_3^-$  accounts for 22%, 27% and 26% of  $\text{PM}_{2.5}$  in the  $\text{PM}_{2.5}$ -of megacities in China (Zong et al., 2020), Europe (Espina-Martin et al., 2024) and U.S. (Sun et al., 2022), respectively. In addition, some studies found that the contribution of  $\text{NO}_3^-$  would increase by 3-8 times with the occurrence of the particular-derived haze pollution (Ge et al., 2024; Song et al., 2019; Yin et al., 2022; Walters et al., 2024).

It is well-known that atmospheric  $\text{NO}_3^-$  is formed by the oxidation of nitrogen oxides ( $\text{NO}_x = \text{NO} + \text{NO}_2$ ) with different oxidants such as  $\text{O}_3$ , OH and  $\text{RO}_2$  (Text S1). In general, atmospheric chemical transportation models are employed to depict the detailed oxidation pathways of  $\text{NO}_3^-$  formation. However, there remains considerable uncertainty in modelling the contribution of individual oxidation pathways to  $\text{NO}_3^-$  formation, particularly the  $\text{N}_2\text{O}_5 + \text{H}_2\text{O}$  pathway, due to the wide variability of key parameters such as the  $\text{N}_2\text{O}_5$  uptake coefficient, which has been shown to vary significantly depending on aerosol composition, relative humidity, and temperature.~~However, there are a large uncertainty in modeling the contribution of oxidation pathways to  $\text{NO}_3^-$  formation using this methodology due to the variable parameters in the real atmosphere.~~ For example, it was reported that the predicted  $\text{N}_2\text{O}_5$  uptake to  $\text{NO}_3^-$  formation in Beijing, as estimated using WRF-Chem, ranges from 5% to 21% (Su et al., 2017). Higher contributions between 66% and 85% have been observed when applying the CMAQ model in Beijing (Qiu et al., 2019). Therefore, the application of alternative techniques is crucial for providing more reliable estimates and enhancing our understanding of  $\text{NO}_3^-$  formation mechanisms, in addition to the insights gained from atmospheric chemical transportation models.

Stable oxygen isotope anomaly ( $\Delta^{17}\text{O} = \delta^{17}\text{O} - 0.52 \times \delta^{18}\text{O}$ ) is recognized as a powerful tool to track formation pathways of atmospheric  $\text{NO}_3^-$  (Zhang et al., 2024; Feng et al., 2023). This is because the oxygen atoms in the terminal positions of  $\text{O}_3$  exhibit an elevated  $\Delta^{17}\text{O}$  ( $\Delta^{17}\text{O} = 39 \pm 2\text{‰}$ ) (Vicars

and Savarino, 2014), whereas the  $\Delta^{17}\text{O}$  values of other atmospheric oxidants (e.g.,  $\text{H}_2\text{O}$ ,  $\text{OH}$ , and  $\text{RO}_2$ ) that can be incorporated to  $\text{NO}_3^-$  are very close to 0‰. (Dubey et al., 1997; Barkan and Luz, 2003; Alexander et al., 2020) Therefore,  $\Delta^{17}\text{O}(\text{NO}_3^-)$  serves as a unique tracer of  $\text{O}_3$  involvement in its formation pathways, offering valuable insights into the relative contributions of individual reactions. In recent years, the use of  $\Delta^{17}\text{O}(\text{NO}_3^-)$  to elucidate  $\text{NO}_3^-$  formation has garnered considerable attention. Walters et al. (2024) reported that the major formation pathways of annual  $\text{HNO}_3$  production in the northeastern U.S. ~~are~~ were  $\text{NO}_2 + \text{OH}$  (46%),  $\text{N}_2\text{O}_5$  uptake (34%), and organic nitrate hydrolysis (12%), with notable seasonal variability. Additionally, Zhang et al. (2022) observed that the contribution of nocturnal chemistry to  $\text{NO}_3^-$  formation ~~increases~~ increased at night, peaking at 72% around midnight. In contrast, the contribution of  $\text{NO}_2 + \text{OH}$  ~~rises~~ rose with sunrise, reaching its highest fraction (48%) around noon. However, nearly all current  $\Delta^{17}\text{O}$ -related observations have been conducted in the plain cities, with little attention given to plateau cities, where atmospheric conditions generally suffer from distinct energy consumption patterns and unique climatic factors (e.g., intense solar radiation). In this study, we present detailed results from comprehensive field observations conducted in Lhasa (3650 m a.s.l), one of the highest cities in the world, located on the Tibetan Plateau, China. For the first time, we quantify the relative contribution of three oxidation pathways to  $\text{NO}_3^-$  formation in Lhasa on the basis of ambient measurements for  $\Delta^{17}\text{O}$  signatures in  $\text{NO}_3^-$ .

## 2. Materials and methods

### 2.1 Sampling campaign

$\text{PM}_{2.5}$  samples were collected on the roof of a building (~15 m above ground) at the Meteorological Bureau of Lhasa (91.08°E, 29.40°N; Figure 1) in China. Lhasa, the capital of the Tibet Autonomous Region, is a rapidly developing city with a population of ~ 950000 and an urban area of ~ 30000 km<sup>2</sup> (Lhasa). The sampling site is surrounded by mixed land use, including residential areas, government offices, religious temples and commercial zones, with minimal heavy industry. The strong solar radiation and large diurnal temperature variations in this sampling site can lead to pronounced changes in boundary layer height, which in turn significantly influence vertical mixing and the transport of air pollutants. ~~This site is located in Chengguan, a typical urban area of Lhasa characterized by a dense population and nearby temples.~~



The sampling campaign was conducted from June 2022 to July 2023 using a high-volume PM<sub>2.5</sub> sampler, which operated at a flow rate of 1.0 m<sup>3</sup>/min. Samples were collected once a week, with each sampling session lasting 48 hours, except during intensive sampling periods in the summer (June 30 to July 14, 2022) and winter (January 28 to February 7, 2023). During these intensive periods, each sample was collected for 12 hours, from 8:00 to 20:00 and 20:00 to 8:00 on the following day, respectively. During the autumn of 2022, Lhasa experienced intermittent COVID-19 control measures, including restricted movement, reduced traffic activity, and temporary lockdowns in urban areas (Daily). Before sampling, all quartz filters (8 in. × 10 in., Pallflex) were calcined in a muffle furnace at 450 °C for 6 h to prevent impurities from contaminating the collected PM<sub>2.5</sub> samples. After sampling, the samples were collected and stored in a freezer at -20°C.

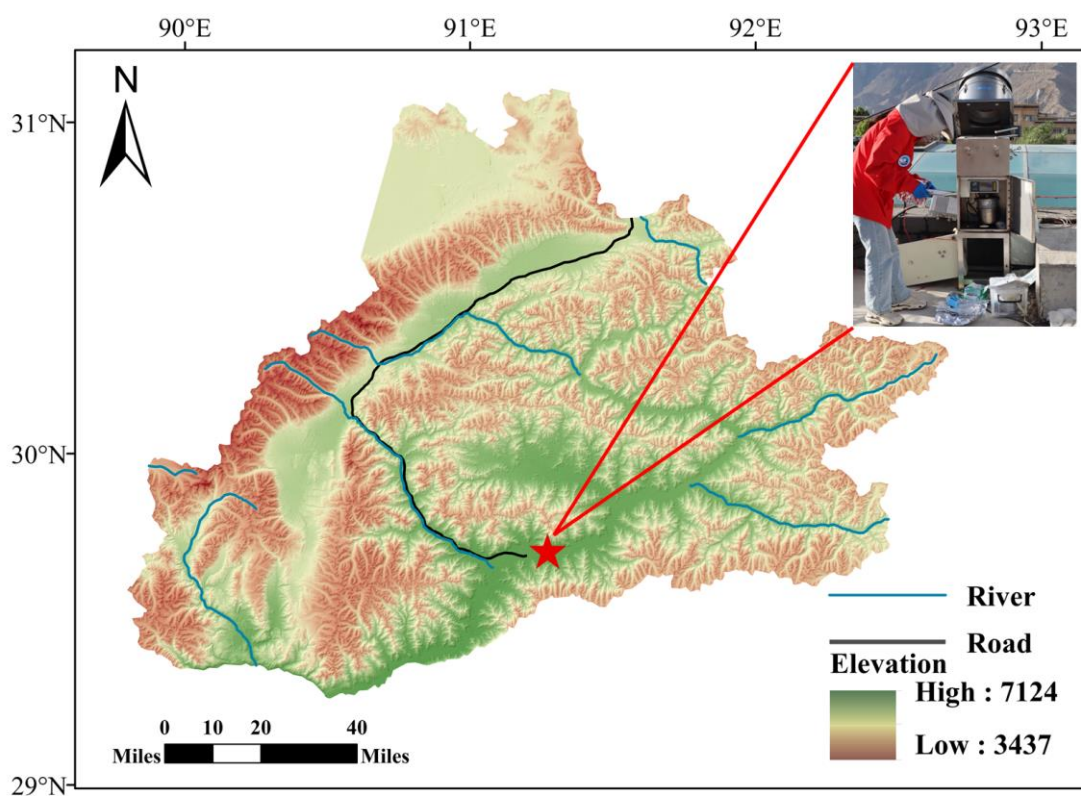


Figure 1. Geographic position of sampling site in Lhasa, China.

## 2.2 Measurements of water-soluble ions and isotopes

Water-soluble ions were measured by an ion chromatography (Dionex ICS-5000, Thermo Scientific Inc.) (Chen et al., 2022). In brief, a part of filter membranes (4.54 cm<sup>2</sup>) was cut using a 17 mm diameter punch and placed in a 15 mL centrifuge tube with 10 mL of 18.2 MΩ ultrapure water. The tube was then subjected to ultrasonic treatment in an ice-water bath for 30 min to prevent ion

volatilization. The extract was filtered through a 0.22  $\mu\text{m}$  filter into a 30 mL sample bottle. This process was repeated with an additional 10 mL of water to ensure full extraction. The final extract was analyzed by an ion chromatography. The method detection limits (MDLs) ~~of for  $\text{Cl}^-$ ,  $\text{NO}_3^-$ ,  $\text{SO}_4^{2-}$ ,  $\text{Na}^+$ ,  $\text{NH}_4^+$ ,  $\text{K}^+$ ,  $\text{Mg}^{2+}$ , and  $\text{Ca}^{2+}$  were 0.0030.001 mg/L, 0.001 mg/L, 0.003 mg/L, 0.02 mg/L, 0.01 mg/L, 0.02 mg/L, 0.006 mg/L, and 0.02 mg/L, respectively.~~

Stable oxygen isotopes ( $\delta^{17}\text{O}$ ,  $\delta^{18}\text{O}$ ,  $\Delta^{17}\text{O}$ , and  $\Delta^{17}\text{O} = \delta^{17}\text{O} - 0.52 \times \delta^{18}\text{O}$ ) of  $\text{NO}_3^-$  were determined using an isotope ratio mass spectrometer (MAT253, Thermo Fisher Scientific, USA) at Nanjing University of Information Science and Technology (Fan et al., 2021; Zhang et al., 2022). Briefly,  $\text{NO}_3^-$  from filter extractions (containing at least 0.8  $\mu\text{g}$  N) ~~was~~were converted into gaseous  $\text{N}_2\text{O}$  using the bacterial denitrifier method.  $\text{N}_2\text{O}$  was then further thermally decomposed into  $\text{O}_2$  and  $\text{N}_2$  in a gold tube heated to 800°C. The produced  $\text{O}_2$  was analyzed for oxygen isotopes by isotope ratio mass spectrometer. The duplicated analysis showed that the errors were within 1.32% for  $\Delta^{17}\text{O}-\text{NO}_3^-$ .

### 2.3 Primary data sources

Meteorological parameters, including ambient temperature (T), relative humidity (RH), rainfall, radiation, wind direction (WD) and wind speed (WS) during the sampling campaign, were obtained from the Meteorological Bureau of Lhasa. Additionally,  $\text{NO}_2$  and  $\text{O}_3$  during the sampling campaign were downloaded from the National Meteorological Information Center (<https://air.cnemc.cn:18007/>~~http://air.cnem.cn:18007/~~).

### 2.4 Evaluation of $\text{NO}_3^-$ oxidation pathways

In our study, we aimed to quantify the relative contribution of different oxidation pathways to  $\text{NO}_3^-$  production based on  $\Delta^{17}\text{O}-\text{NO}_3^-$ . Due to the low  $\text{Cl}^-$  concentrations observed in Lhasa, the  $\text{NO}_3^-$  formation pathways considered in this study are limited to  $\text{NO}_2 + \text{OH}$ ,  $\text{NO}_3 + \text{VOC}$ , and  $\text{N}_2\text{O}_5 + \text{H}_2\text{O}$ . Although  $\text{NO}_3 + \text{VOC}$  was generally considered a minor pathway in continental regions (Alexander et al., 2009), we included it because elevated VOC concentrations were observed at our sampling site in Lhasa, influenced by both biogenic emissions (e.g. incense burning) and anthropogenic sources (e.g. vehicle emissions) (Tang et al., 2022). The relative contributions of the three pathways were determined using a  $\Delta^{17}\text{O}$ -based mass balance approach (Michalski et al., 2003), as shown in Equations (1) and (2):

$$\Delta^{17}\text{O}-\text{NO}_3^- = (\Delta^{17}\text{O}-\text{NO}_3^-)_{\text{NO}_2+\text{OH}} \times f_{\text{NO}_2+\text{OH}} + (\Delta^{17}\text{O}-\text{NO}_3^-)_{\text{NO}_3+\text{VOC}} \times f_{\text{NO}_3+\text{VOC}} + (\Delta^{17}\text{O}-\text{NO}_3^-)_{\text{N}_2\text{O}_5+\text{H}_2\text{O}} \times f_{\text{N}_2\text{O}_5+\text{H}_2\text{O}} \quad (1)$$



$$f_{\text{NO}_2+\text{OH}} + f_{\text{NO}_3+\text{VOC}} + f_{\text{N}_2\text{O}_5+\text{H}_2\text{O}} = 1 \quad (2)$$

where  $\Delta^{17}\text{O}-\text{NO}_3^-$  value is the  $\Delta^{17}\text{O}$  value of  $\text{NO}_3^-$  in  $\text{PM}_{2.5}$ . The  $(\Delta^{17}\text{O}-\text{NO}_3^-)_{\text{NO}_2+\text{OH}}$ ,  $(\Delta^{17}\text{O}-\text{NO}_3^-)_{\text{NO}_3+\text{VOC}}$ , and  $(\Delta^{17}\text{O}-\text{NO}_3^-)_{\text{N}_2\text{O}_5+\text{H}_2\text{O}}$  correspond to the  $\Delta^{17}\text{O}$  values from  $\text{NO}_2+\text{OH}$ ,  $\text{NO}_3+\text{VOC}$  and  $\text{N}_2\text{O}_5+\text{H}_2\text{O}$ , respectively. The  $\Delta^{17}\text{O}$  values for each pathway were calculated using Equations (3), (4), and (5) (Savarino et al., 2016; Alexander et al., 2009):

$$(\Delta^{17}\text{O}-\text{NO}_3^-)_{\text{NO}_2+\text{OH}} (\%) = 2/3\alpha \times \Delta^{17}\text{O}-\text{O}_3^* \quad (3)$$

$$(\Delta^{17}\text{O}-\text{NO}_3^-)_{\text{NO}_3+\text{VOC}} (\%) = 2/3\alpha \times \Delta^{17}\text{O}-\text{O}_3^* + 1/3 \times \Delta^{17}\text{O}-\text{O}_3^* \quad (4)$$

$$(\Delta^{17}\text{O}-\text{NO}_3^-)_{\text{N}_2\text{O}_5+\text{H}_2\text{O}} (\%) = 1/3\alpha \times \Delta^{17}\text{O}-\text{O}_3^* + 1/2(2/3\alpha \times \Delta^{17}\text{O}-\text{O}_3^* + 1/3 \times \Delta^{17}\text{O}-\text{O}_3^*) \quad (5)$$

Previous studies have demonstrated a linear correlation between  $\Delta^{17}\text{O}-\text{O}_3$  and  $\Delta^{17}\text{O}-\text{O}_3^*$ , with  $\Delta^{17}\text{O}(\text{O}_3)$  values ranging from 20% to 40% in tropospheric  $\text{O}_3$  (Vicars and Savarino, 2014; Ishino et al., 2017). The equations are shown as follows (Vicars et al., 2012):

$$\Delta^{17}\text{O}-\text{O}_3^* = 1.5 \times \Delta^{17}\text{O}-\text{O}_3 \quad (6)$$

Based on previous observations of tropospheric  $\text{O}_3$ ,  $\Delta^{17}\text{O}-\text{O}_3^*$  average value was approximately 39‰. The  $\alpha$  value represents the proportional contribution of  $\text{O}_3$  to the  $\text{NO}$  oxidation pathway and can be estimated using the following equations (7) (Alexander et al., 2009). When  $\text{NO}_x$  is in photochemical steady state,  $\Delta^{17}\text{O}-\text{NO}_2$  can be represented using the following equation (10):

$$\alpha = K_{\text{P1}} [\text{O}_3] \times [\text{NO}] / (K_{\text{P1}} [\text{O}_3] \times [\text{NO}] + K_{\text{P2}} [\text{NO}] \times [\text{HO}_2] + K_{\text{P3}} [\text{NO}] \times [\text{RO}_2]) \quad (7)$$

$$K_{\text{P1}} = 3.0 \times 10^{-12} \times e^{(-1500/T)} \quad (8)$$

$$K_{\text{P2}} = K_{\text{P3}} = 3.5 \times 10^{-12} \times e^{(270/T)} (\text{cm}^3 \cdot \text{molecule}^{-1} \cdot \text{s}^{-1}) \quad (9)$$

$$\Delta^{17}\text{O}-\text{NO}_2 = \alpha \Delta^{17}\text{O}-\text{O}_3^* \quad (10)$$

where  $T$  represents the ambient temperature (K) (Kunasek et al., 2008). The  $\text{HO}_2$  mixing ratios were estimated using empirical equations in the absence of direct  $\text{HO}_2$  observations (Kanaya et al., 2007). Due to the lower temperatures in Lhasa during non-summer seasons,  $\text{HO}_2$  concentrations were assessed using a formula derived from winter conditions.

#### Winter

$$[\text{HO}_2 \cdot] / \text{ppt} = \exp(5.7747 \times 10^{-2} [\text{O}_3] (\text{ppb}) - 1.7227) \text{ for daytime} \quad (11)$$

$$[\text{HO}_2 \cdot] / \text{ppt} = \exp(7.7234 \times 10^{-2} [\text{O}_3] (\text{ppb}) - 1.6363) \text{ for nighttime} \quad (12)$$

#### Summer

$$[\text{HO}_2 \cdot] / \text{pptv} = \exp(2.0706 \times 10^{-2} [\text{O}_3] (\text{ppb}) + 1.0625) \text{ for daytime} \quad (13)$$

$$[\text{HO}_2 \cdot] / \text{pptv} = 0.2456 + 0.1841 [\text{O}_3] (\text{ppb}) \text{ for nighttime} \quad (14)$$

## 2.4.5 Stable isotope analysis in the R (SIAR) model

In this study, stable isotope analysis in the R (SIAR) model was employed to estimate the relative contributions of three main pathways to  $\text{NO}_3^-$  (Parnell et al., 2010). The SIAR model is well-suited for analyzing multiple formation pathways, as it effectively incorporates uncertainties and parameter variability, leading to more reliable estimates. Specifically, this model allows for a detailed analysis of oxygen isotope ( $\Delta^{17}\text{O}$ ), enabling accurate modeling of  $\text{NO}_3^-$  formation pathways based on oxygen isotope measurements. The SIAR model is a Bayesian mixture model, mathematically formulated as follows:

$$X_i = \sum_{j=1}^K p_j \times f_{ij}$$

$$p_1 + p_2 + \dots + p_k = 1$$

$$f_{ij} \sim N(\mu_j, \omega_j^2)$$

Where  $X_i$  is the observed  $\Delta^{17}\text{O}$  values for sample  $i$  ( $i = 1, 2, 3, \dots, N$ ) and  $p_j$  is the proportional contribution of each  $\text{NO}_3^-$  formation pathway  $j$  to the sample  $i$ .  $f_{ij}$  is the  $\Delta^{17}\text{O}$  values of formation pathway  $j$  for sample  $i$  and follows a normal distribution with mean ( $\mu_j$ ) and variance ( $\omega_j^2$ ). Within the Bayesian framework, prior distributions are assigned to each  $p_j$ , and these are updated with the observed data  $X_i$  to obtain posterior distributions, allowing for inference of the proportional contributions  $p_j$  of each pathway.

## 2.5–6 Aerosol liquid water content (ALWC) and the Hybrid Single-Particle Lagrangian Integrated Trajectory (HYSPLIT)

To evaluate the influence of ~~aerosol liquid water content~~ (ALWC) on the  $\text{NO}_3^-$  formation, ALWC was calculated using the ISORROPIA II model developed by Fountoukis and Nenes (Fountoukis and Nenes, 2007). The ISORROPIA II model includes two modes: the forward mode, which requires the concentrations of both particulate and gaseous pollutants concentrations as inputs, and the reverse mode, which only requires the concentrations of particulate pollutants concentrations. The model computes the ALWC in both modes based on particulate pollutant concentrations (e.g.,  $\text{NH}_4^+$ ,  $\text{Na}^+$ ,  $\text{Ca}^{2+}$ ,  $\text{K}^+$  and  $\text{Mg}^{2+}$ ), as well as ambient RH and T. In this study, the reverse mode was employed due to the lack of gaseous pollutant concentrations observations.

Additionally, the Hybrid Single-Particle Lagrangian Integrated Trajectory (HYSPLIT) model was

utilized to compute 72-hours back trajectories during the sampling campaign. HYSPLIT, developed by the National Oceanic and Atmospheric Administration Air Resources Laboratory (NOAA/ARL), is available on the their website (<https://www.ready.noaa.gov/HYSPLIT.php>~~http://www.arl.noaa.gov/ready/hysplit4.html~~), ~~—~~). This model has been widely used for simulating the transport and dispersion trajectories of pollutants such as PM<sub>2.5</sub>, VOC<sub>s</sub>, O<sub>3</sub>, and NO<sub>x</sub>, among others (He et al., 2022; Zhao et al., 2015; Cao et al., 2023). Backward trajectories for each sampling day were calculated at an altitude of 3650 meters using meteorological data from the Global Data Assimilation System (GDAS), available through the US Air Resources Laboratory (NOAA ARL) (<https://www.ready.noaa.gov/data/archives/gdas1/>).

### 3. Results

#### 3.1 Overview of the meteorological parameters in Lhasa during the sampling campaign

Figure 2a presents the daily variations in meteorological parameters, including temperature, relative humidity (RH), rainfall and solar radiation. During the sampling campaign, the annual average temperature was 11.5°C, ranging from -2.83 to 24.2°C. The highest average temperature was observed in summer (19.7°C), while the lowest (3.11°C) was recorded in winter. Relative humidity (RH) varied between 6.67 and 66.8%, with the lowest average RH occurring in winter (17.1%) and the highest in summer (35.6%). The near-surface layer of Lhasa is influenced by a thermal low-pressure system, and the southwest monsoon, active between June and September, transports moisture-laden air from the Indian Ocean, resulting in increased rainfall during summer. Solar radiation intensity exhibited a seasonal trend ~~consistent~~<sup>opposite</sup> to those of temperature and RH, peaking in summer (394 W/m<sup>2</sup>) and reaching its lowest levels in winter (220 W/m<sup>2</sup>). The dominant wind direct (WD) was southeast in spring, but southwest in the other three seasons (Figure 3). Wind speed (WS) was highest in spring but lowest in autumn.

#### 3.2 NO<sub>3</sub><sup>-</sup> concentration

NO<sub>3</sub><sup>-</sup> mass concentrations ranged from 0.10 to 1.72 µg/m<sup>3</sup>, with an average value of 0.62 ± 0.31 µg/m<sup>3</sup>. NO<sub>3</sub><sup>-</sup> concentrations exhibited distinct seasonal patterns. As shown in Figure S1, the equivalent concentrations of [SO<sub>4</sub><sup>2-</sup> + NO<sub>3</sub><sup>-</sup>] were considerably higher than those of [NH<sub>4</sub><sup>+</sup>], indicating that NH<sub>4</sub><sup>+</sup> was insufficient to fully neutralize NO<sub>3</sub><sup>-</sup>. This suggests that a portion of NO<sub>3</sub><sup>-</sup> may have existed in other

forms, such as  $\text{KNO}_3$  and  $\text{Ca}(\text{NO}_3)_2$ . This inference is supported by the strong positive correlations between  $\text{NO}_3^-$  and  $\text{K}^+$  ( $r = 0.64$ ,  $p < 0.1$ ) and  $\text{Ca}^{2+}$  ( $r = 0.43$ ,  $p < 0.01$ ), especially in spring, as shown in Figure S2. In contrast,  $\text{NO}_3^-$  showed relatively weak negative correlations with T ( $r = -0.27$ ,  $p < 0.01$ ) and RH ( $r = -0.22$ ,  $p < 0.1$ ), indicating that under the specific atmospheric conditions in Lhasa, meteorological parameters might not be the dominant factors controlling the gas-particle partitioning of  $\text{NO}_3^-$ . Specifically, the maximum monthly average values of  $\text{NO}_3^-$  concentration occurred in spring ( $0.83 \pm 0.35 \mu\text{g}/\text{m}^3$ ) with the instantaneous maximum reaching  $1.72 \mu\text{g}/\text{m}^3$ , whereas the lowest was recorded in autumn ( $0.23 \pm 0.13 \mu\text{g}/\text{m}^3$ ) with an instantaneous minimum of only  $0.09 \mu\text{g}/\text{m}^3$  (Table 1). The elevated  $\text{NO}_3^-$  concentrations in spring could be attributed to biomass burning emitted from south and Southeast Asia (Figure S3/Figure S4). The strong between  $\text{NO}_3^-$  and  $\text{K}^+$  in spring further this explanation. The difference in  $\text{NO}_3^-$  concentrations between autumn and other three seasons was statistically significant ( $p < 0.05$ ). The considerable seasonal variation in  $\text{NO}_3^-$  concentrations in Lhasa is associated with varying emission sources and meteorological conditions.

In spring, high  $\text{NO}_3^-$  concentrations were associated with weak southeasterly winds ( $< 3 \text{ m/s}$ ) in the bivariate polar plot, suggesting probable impacts from local/regional emissions (Figure 3). The southeasterly sector of sampling site includes residential areas, agriculture land and major transportation routes, which are potential  $\text{NO}_x$  sources. In spring, intensified agriculture activities (e.g., fertilization, biomass burning) might increase  $\text{NO}_x$  emissions. Meanwhile, low wind speeds likely limit atmospheric dispersion, promoting the local accumulation of precursors and enhancing  $\text{NO}_3^-$  production. During the rainy summer, shorter  $\text{NO}_3^-$  lifetimes indicated a weak influence from regional transport, with a more pronounced contribution from local/regional emissions. In autumn,  $\text{NO}_3^-$  concentrations were relatively low, which coincided with strict local COVID-19 restrictions in Lhasa. These measures significantly reduced human activity and traffic, leading to suppressed local emissions, partly due to the reduced local emissions caused by the COVID-19 pandemic, which led to decreased human activity and transportation. Despite low wind speeds typically favor pollutant accumulation,  $\text{NO}_3^-$  concentrations remained low, suggesting that both reduced local sources and seasonal meteorological conditions constrained  $\text{NO}_3^-$  production. Nevertheless, the persistence of measurable  $\text{NO}_3^-$  under such stagnant conditions also implied a potential contribution from regional transport during this period. The lower  $\text{NO}_3^-$  levels during this period suggest that the pandemic, combined with seasonal meteorological conditions, played a role in limiting local/regional emissions.

281 In winter, elevated  $\text{NO}_3^-$  concentrations under low wind speeds ( $< 3$  m/s) emphasized~~d~~ the significant  
282 contribution of local/~~regional~~ emissions. These findings underscore~~d~~ that,~~in addition to~~ both regional  
283 transport and, local emissions ~~are~~were ~~the primary~~important contributors~~s~~ to  $\text{NO}_3^-$  concentrations in  
284 Lhasa,~~especially under low wind conditions, with the pandemic further influencing local emission~~  
285 ~~levels~~. Furthermore, based on our day-night sampling scheme, no nycthemeral (day-night)  
286 differences in  $\text{NO}_3^-$  concentrations were detected (Table S1). A similar day-night pattern of  $\text{NO}_3^-$   
287 concentrations also has been observed in in Beijing (Luo et al., 2020).



288 Table 1 Average values of water-soluble ions and  $\Delta^{17}\text{O-NO}_3^-$  during the sampling campaign

289

		$\text{Na}^+$	$\text{NH}_4^+$	$\text{K}^+$	$\text{Mg}^{2+}$	$\text{Ca}^{2+}$	$\text{Cl}^-$	$\text{NO}_3^-$	$\text{SO}_4^{2-}$	$\Delta^{17}\text{O-NO}_3^-$
		$\mu\text{g/m}^3$	$\mu\text{g/m}^3$	$\mu\text{g/m}^3$	$\mu\text{g/m}^3$	$\mu\text{g/m}^3$	$\mu\text{g/m}^3$	$\mu\text{g/m}^3$	$\mu\text{g/m}^3$	‰
<b>Annual</b>	<b>Minmum</b>	0.02	0	0.004	0.004	0.004	0.004	0.09	0.06	18.3
	<b>Maximum</b>	0.68	1.22	0.29	0.08	3.52	0.51	1.72	2.37	34.1
	<b>Average</b>	0.16	0.3	0.07	0.02	1.09	0.08	0.62	0.74	26.3
	<b>Std.Dev</b>	0.14	0.26	0.06	0.01	0.7	0.1	0.31	0.45	3.13
<b>spring</b>	<b>Minmum</b>	0.04	0.16	0.04	0.01	1.02	0.01	0.45	0.6	27.2
	<b>Maximum</b>	0.16	1.22	0.2	0.05	2.56	0.05	1.72	2.14	30.4
	<b>Average</b>	0.09	0.52	0.09	0.02	1.67	0.03	0.83	1.11	28.8
	<b>Std.Dev</b>	0.03	0.3	0.04	0.01	0.51	0.01	0.35	0.52	0.99
<b>summer</b>	<b>Minmum</b>	0.02	0	0.01	0.01	0.03	0.003	0.13	0.18	20.2
	<b>Maximum</b>	0.4	1.08	0.09	0.04	2.4	0.13	1	2.37	28.5
	<b>Average</b>	0.09	0.18	0.03	0.02	1.15	0.3	0.5	0.72	25.5
	<b>Std.Dev</b>	0.08	0.17	0.02	0.01	0.5	0.3	0.23	0.45	2.2
<b>autumn</b>	<b>Minmum</b>	0.02	0.003	0.004	0.01	0.004	0.01	0.09	0.06	21.2
	<b>Maximum</b>	0.17	0.11	0.1	0.03	0.24	0.17	0.51	0.55	24.9
	<b>Average</b>	0.09	0.04	0.3	0.02	0.13	0.05	0.23	0.31	23.05
	<b>Std.Dev</b>	0.05	0.04	0.3	0.01	0.08	0.05	0.13	0.14	1.44
<b>winter</b>	<b>Minmum</b>	0.06	0.09	0.02	0.01	0.05	0.04	0.21	0.32	18.3
	<b>Maximum</b>	0.56	0.87	0.29	0.08	3.52	0.51	1.46	1.57	34.1
	<b>Average</b>	0.19	0.44	0.12	0.03	1.04	0.16	0.75	0.73	25.9
	<b>Std.Dev</b>	0.12	0.21	0.08	0.02	0.78	0.13	0.28	0.34	3.86

290

291

292

### 3.3 Oxygen isotopes of $\text{NO}_3^-$

To explore the three major oxidation pathways of  $\text{NO}_3^-$  formation, 53 samples representing varying  $\text{NO}_3^-$  concentrations across different seasons were selected for oxygen isotope measurements (Figure 2b). The  $\Delta^{17}\text{O}-\text{NO}_3^-$  values ranged from 18.3 to 34.1‰, with an average of  $26.3 \pm 3.13\text{‰}$ , which is slightly lower than the global average of  $28.6 \pm 4.5\text{‰}$  simulated by the Global Chemical Transport Model (Alexander et al., 2020). As shown in Table S3S2, the observed  $\Delta^{17}\text{O}-\text{NO}_3^-$  values in this study were similar to most mid- and low-latitude regions, but lower than those in polar regions ( $\sim 32\text{‰}$ ). ~~Clear seasonal variations in  $\Delta^{17}\text{O}-\text{NO}_3^-$  values were seen in Lhasa (Figure 2b).~~ As listed in Table S1, the average  $\Delta^{17}\text{O}-\text{NO}_3^-$  values in spring, summer, autumn and winter were  $28.8 \pm 8.0\text{‰}$ ,  $25.5 \pm 2.20\text{‰}$ ,  $25.6 \pm 1.35\text{‰}$ , and  $25.9 \pm 3.56\text{‰}$ , respectively. The differences in  $\Delta^{17}\text{O}-\text{NO}_3^-$  values between spring and summer, as well as between spring and winter, were statistically significant ( $p < 0.05$ ). The elevated  $\Delta^{17}\text{O}-\text{NO}_3^-$  values in spring could be attributed to a higher proportion of nocturnal pathways that enrich  $\Delta^{17}\text{O}-\text{NO}_3^-$  values, such as  $\text{NO}_3 + \text{VOC}$  and  $\text{N}_2\text{O}_5 + \text{H}_2\text{O}$  pathway. In contrast, the lower  $\Delta^{17}\text{O}-\text{NO}_3^-$  values in other three seasons suggested a greater production of  $\text{NO}_3^-$  formation via  $\text{NO}_2 + \text{OH}$  pathway, leading to more negative  $\Delta^{17}\text{O}-\text{NO}_3^-$  values. Diurnal variation in  $\Delta^{17}\text{O}-\text{NO}_3^-$  values also differed across season (Figure S5). In summer, the average of  $\Delta^{17}\text{O}-\text{NO}_3^-$  values during the day ( $25.3 \pm 2.39\text{‰}$ ) was lower than at night ( $26.7 \pm 1.03\text{‰}$ ). Conversely, in winter, the average of  $\Delta^{17}\text{O}-\text{NO}_3^-$  values during the day ( $28.0 \pm 3.79\text{‰}$ ) was significantly higher than at ~~the nightnight~~ ( $24.4 \pm 3.85\text{‰}$ ). Similar diurnal patterns, with higher daytime  $\Delta^{17}\text{O}-\text{NO}_3^-$  values and lower nighttime values, have also been observed in winter in the U.S. (Vicars et al., 2013) and other cities in China (He et al., 2018).

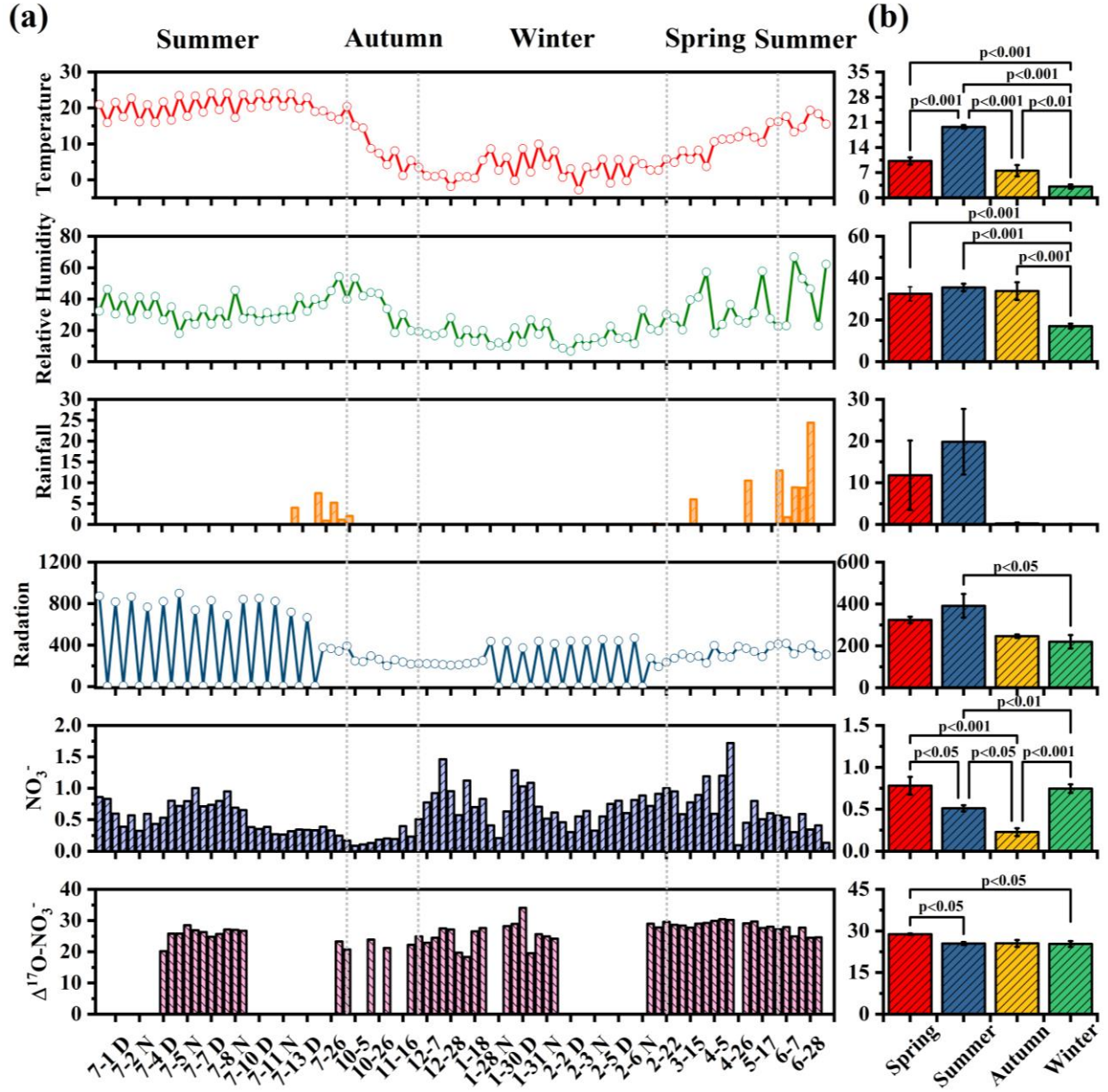
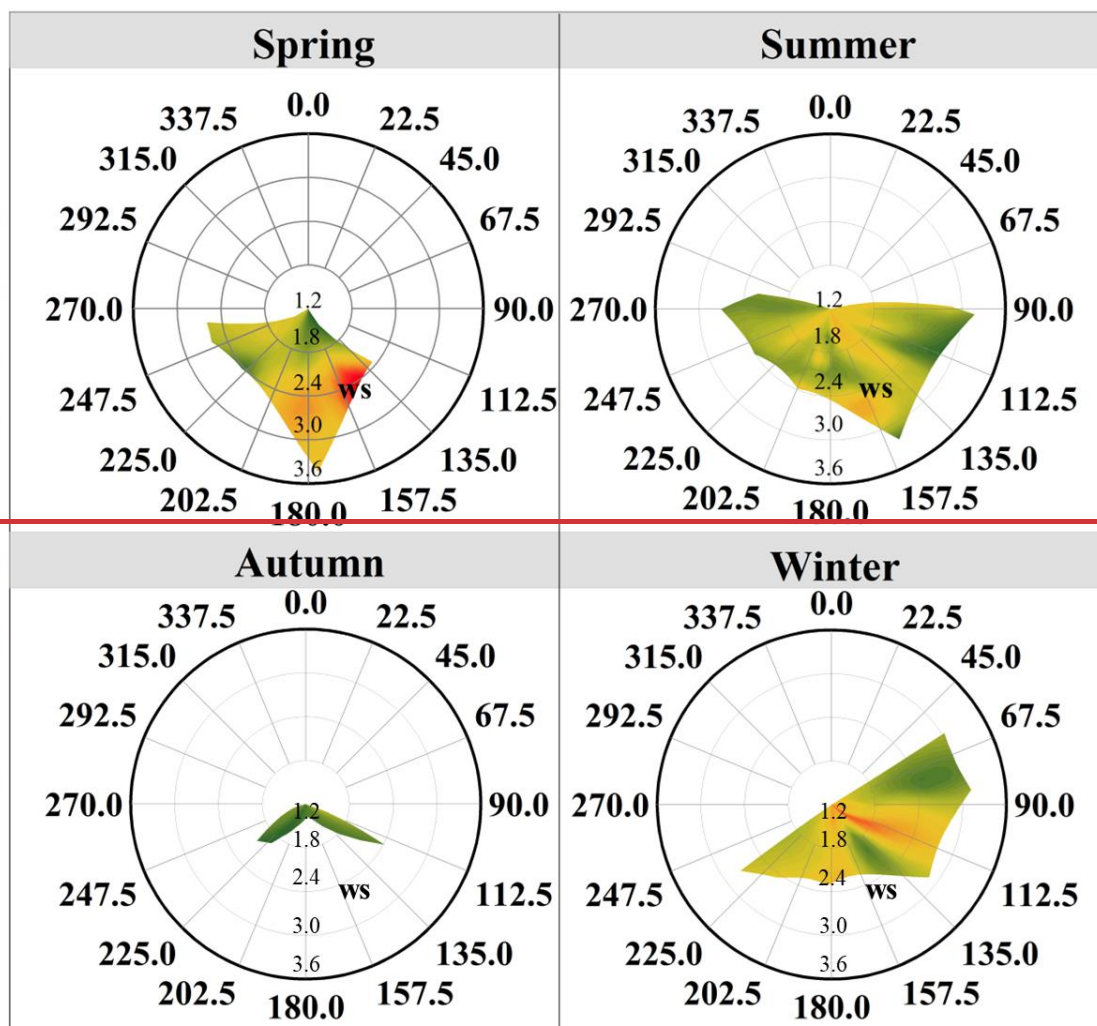
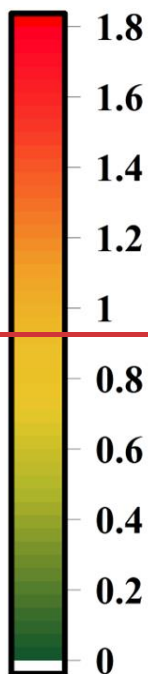


Figure 2. (a) shows the time series of temperature ( $^{\circ}C$ ), relative humidity (%), Rainfall (mm), Radiation ( $W/m^2$ ),  $NO_3^-$  concentration ( $\mu g/m^3$ ), and  $\Delta^{17}O-NO_3^-$  (‰) from June 2022 to July 2023. (b) shows the average values significance at different seasons with their statistical.

$\text{NO}_3^-$   
( $\mu\text{g}/\text{m}^3$ )



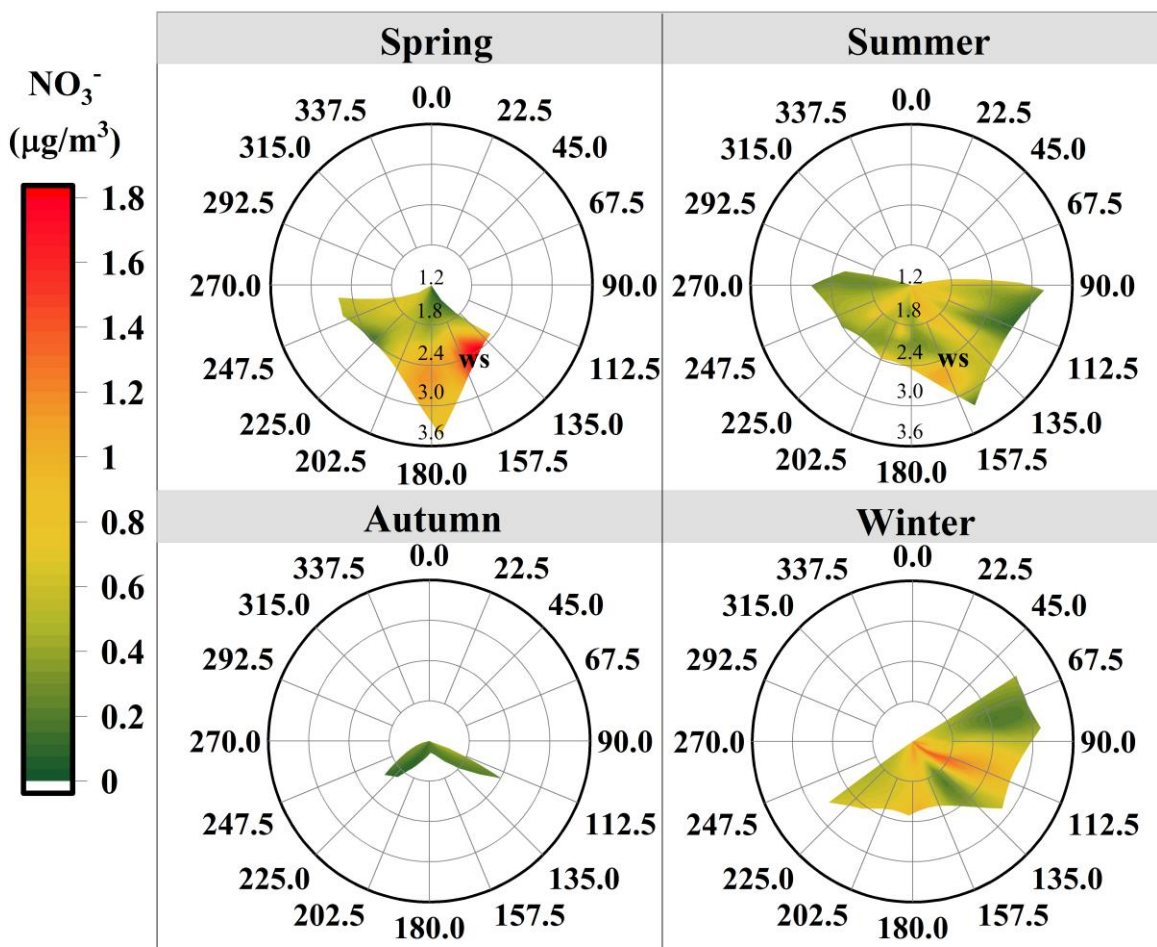


Figure 3. Bivariate polar plot illustrates the seasonal variation in the mass concentration of  $\text{NO}_3^-$  in relation to wind speed (WS, m/s) and wind direction (WD, degrees).

## 4. Discussion

### 4.1 A comparison of $\text{NO}_3^-$ oxidation pathways in Lhasa with other megacities in plain regions

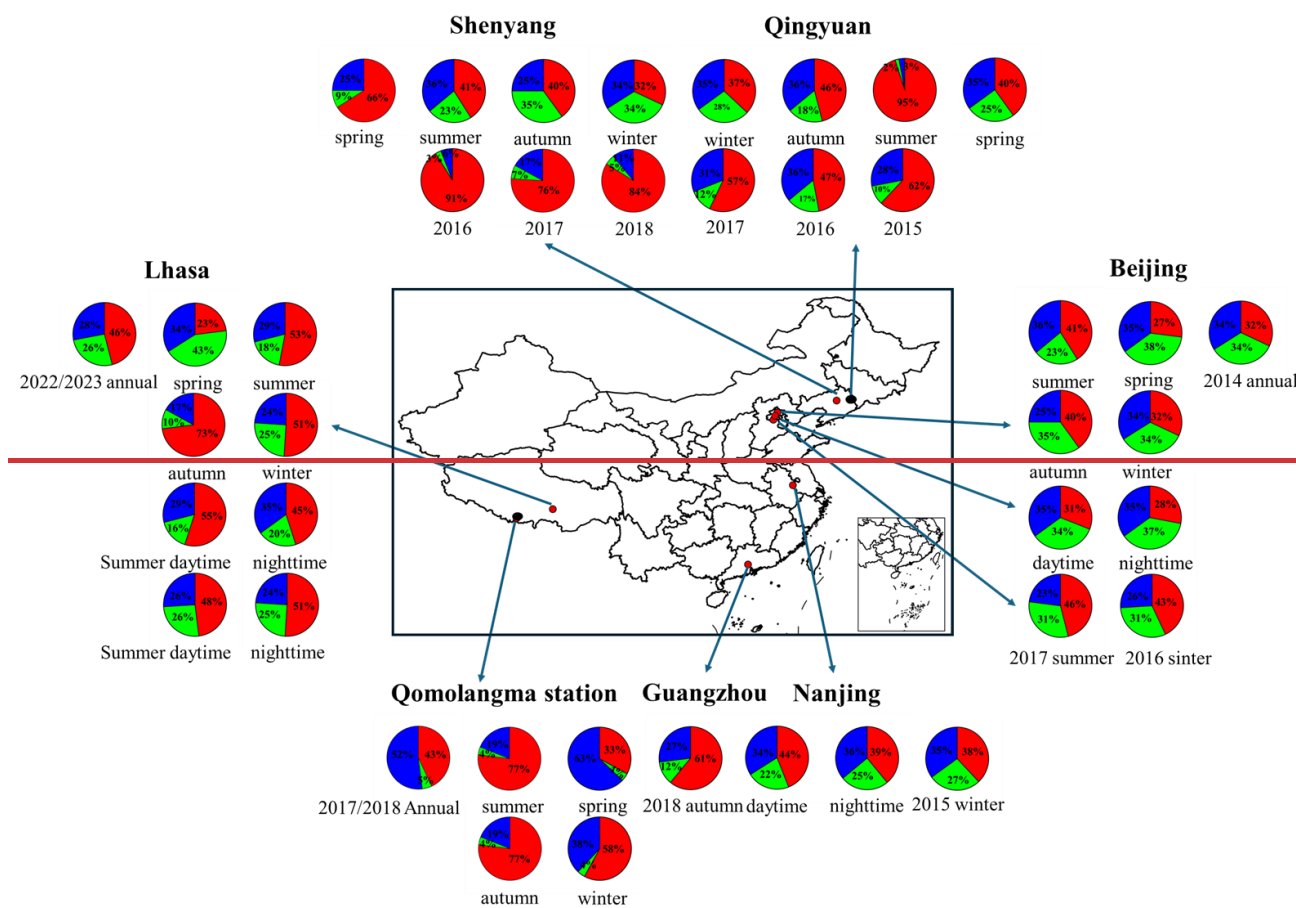
Typically, observations of  $\Delta^{17}\text{O}-\text{NO}_3^-$  and estimated  $\alpha$  (the proportion of  $\text{O}_3$  oxidation in  $\text{NO}_2$  production rate) values are employed to quantify the contributions of major  $\text{NO}_3^-$  oxidation pathway in conjunction with a Bayesian model. The  $\alpha$  value ranged from 0.63 to 0.93, with an average of  $0.83 \pm 0.06$ , suggesting the significance of  $\text{O}_3$  participation in  $\text{NO}$  oxidation during the sampling campaign. On the other hand, our  $\alpha$  values were lower than those (0.85-1) for other midlatitude regions (Alexander et al., 2009). The  $\alpha$  values are influenced by the relative amount of  $\text{O}_3$ ,  $\text{HO}_2$  and  $\text{RO}_2$  in  $\text{NO}_x$  cycling. Due to the generally high  $\text{O}_3$  concentrations ( $\text{O}_3 > 50$  ppb) observed in Lhasa, nearly all  $\alpha$  values exceeded 0.8 (Figure S6). To evaluate the impact of key parameters on the estimated contributions of different  $\text{NO}_3^-$  formation pathways, we conducted a sensitivity analysis by assumed



the  $\alpha$  values and  $\Delta^{17}\text{O}$  value of the terminal oxygen atoms of  $\text{O}_3$  ( $\Delta^{17}\text{O}-\text{O}_3^*$ ). As listed in Table S3, the assumption of  $\alpha$  and  $\Delta^{17}\text{O}-\text{O}_3^*$  have an impact on the  $\text{NO}_3^-$  formation mechanisms. When  $\Delta^{17}\text{O}-\text{O}_3^*$  was fixed at 39‰, increasing  $\alpha$  from 0.7 to 0.9 led to a notable increase in the relative contribution of the  $\text{NO}_2 + \text{OH}$  pathway from 25% to 46%, while that of the  $\text{NO}_3 + \text{VOC}$  pathway decreased from 46% to 25%. The  $\text{N}_2\text{O}_5 + \text{H}_2\text{O}$  pathway remained nearly constant, with contributions ranging between 28% and 29%, indicating that this pathway is relatively insensitive to changes in  $\alpha$  values. Similarly, when  $\alpha$  was varied within a reasonable range (0.68-0.93), increasing the  $\Delta^{17}\text{O}-\text{O}_3^*$  value from 37‰ to 39‰ led to an increase in the  $\text{NO}_2 + \text{OH}$  contribution from 37% to 46%, and a corresponding decrease in the  $\text{NO}_3 + \text{VOC}$  contribution from 35% to 26%. Again, the  $\text{N}_2\text{O}_5 + \text{H}_2\text{O}$  contribution remained stable at  $\sim 28\%$ . These results suggest that the estimated contributions of  $\text{NO}_2 + \text{OH}$  and  $\text{NO}_3 + \text{VOC}$  pathways are sensitive to assumptions about  $\alpha$  and  $\Delta^{17}\text{O}-\text{O}_3^*$ , whereas the contribution of the  $\text{N}_2\text{O}_5 + \text{H}_2\text{O}$  pathway is relatively robust under the tested conditions. Because Lhasa is characterized by relatively high VOC concentrations and  $\Delta^{17}\text{O}-\text{O}_3^*$  is generally close to 39‰, we consider our parameter assumptions reasonable for further estimating  $\text{NO}_3^-$  formation pathways for each sample, likely due to stronger UV radiation enhancing OH radical production and competitive oxidation pathways involving VOC and  $\text{RO}_2$  in Lhasa.

On average, the relative contributions of  $\text{NO}_2 + \text{OH}$  ( $f_{\text{NO}_2+\text{OH}}$ ),  $\text{NO}_3 + \text{VOC}$  ( $f_{\text{NO}_3+\text{VOC}}$ ) and  $\text{N}_2\text{O}_5 + \text{H}_2\text{O}$  ( $f_{\text{N}_2\text{O}_5+\text{H}_2\text{O}}$ ) to  $\text{NO}_3^-$  formation in Lhasa during the sampling campaign were  $46 \pm 26\%$ ,  $26 \pm 19\%$  and  $28 \pm 11\%$ , respectively. To better understand the characteristics of  $\text{NO}_3^-$  formation mechanism in Lhasa, we performed a detailed comparison around the China for the relative contributions of key oxidation pathways using the  $\Delta^{17}\text{O}$  methodology (Figure 4). Overall, similar to most Chinese cities,  $\text{NO}_3^-$  formation in Lhasa was predominantly driven by the  $\text{NO}_2 + \text{OH}$  pathway, exhibiting distinct seasonal and regional variations. In particular, the average  $f_{\text{NO}_3+\text{VOC}}$  values were generally several times higher in spring in Lhasa than in other urban cities. Compared to rural/remote areas, the average  $f_{\text{NO}_3+\text{VOC}}$  values showed higher fractions in Lhasa, revealing the influence of anthropogenic emission, i.e., vehicle exhaust and heating, on  $\text{NO}_3^-$  formation. In Lhasa, the Capital of Tibet, field measurements among different years showed a substantial increase in VOC concentrations in urban areas of the Tibet Plateau, comparable to those in North China (Tang et al., 2022), revealing the importance of the active  $\text{NO}_3 + \text{VOC}$  pathway for  $\text{NO}_3^-$  pollution formation in Lhasa. In fact, Recent recent studies have emphasized-recognized that  $\text{NO}_3 + \text{VOC}$  is as a major formation mechanism of

for  $\text{NO}_3^-$  production. For instance, Fan et al. (2021) found that  $f_{\text{NO}_3+\text{VOC}}$  in Beijing increased from 17% in summer to 32% in winter based on  $\Delta^{17}\text{O}-\text{NO}_3^-$  measurements. ~~used  $\Delta^{17}\text{O}-\text{NO}_3^-$  to reveal that the average  $f_{\text{NO}_3+\text{VOC}}$  value was 17% in summer and increased to 32% in winter based on  $\Delta^{17}\text{O}-\text{NO}_3^-$  observations in Beijing.~~ He et al. (2018) estimated the relative contributions of  $\text{NO}_3 + \text{VOC}$  and  $\text{N}_2\text{O}_5 + \text{Cl}^-$  to  $\text{NO}_3^-$  formation and found that  $\text{NO}_3 + \text{VOC}$  and  $\text{N}_2\text{O}_5 + \text{Cl}^-$  were in the range of 16-56%, underscoring the significant roles of these pathways during haze events in Beijing. Meanwhile Similarly, Feng et al. (2023) also reported that the  $f_{\text{NO}_3+\text{VOC}}$  values were up to 49.6% in winter in northern China. In Guangzhou, Additionally, Wang et al. (2023) noted that in Guangzhou, the average  $f_{\text{NO}_3+\text{VOC}}$  value was at the 488m (25%) higher than that at the ground (12%). Furthermore, Li et al. (2022) reported that  $f_{\text{NO}_3+\text{VOC}}$  increased from 5% in urban to 13.5% in rural regions in Northeast China, utilized  $\Delta^{17}\text{O}-\text{NO}_3^-$  to explore the oxidation pathway of  $\text{NO}_3^-$  in both urban and rural atmosphere in Northeast China and found that the  $f_{\text{NO}_3+\text{VOC}}$  values increased from 5% in urban areas to 13.5% in rural areas. Although the specific nighttime  $\text{RO}_2$  production mechanism in Lhasa remains unclear, studies in other cities have demonstrated that  $\text{NO}_3+\text{VOC}$  pathway was the dominant channel for nighttime  $\text{RO}_2$  (Fisher et al., 2016), which in turn leads to the formation of alkyl and multifunctional nitrates ( $\text{RONO}_2$ ) and eventually  $\text{NO}_3^-$ . In such cases, the  $\text{RO}_2$  concentration is expected to be correlated with  $\text{NO}_3$  radical production, which depends on the reaction rate of  $\text{O}_3$  and  $\text{NO}_2$  (Brown and Stutz, 2012). Given the relatively high nighttime  $\text{O}_3$  concentrations in Lhasa, it is plausible that  $\text{O}_3$ -driven nighttime  $\text{NO}_3$  chemistry plays an important role, thereby enhancing  $\text{NO}_3+\text{VOC}$  derived from  $\text{RO}_2$  production and  $\text{NO}_3^-$  formation. Global modelling studies also support the significant of this pathway. For instance, Alexander et al. (2020) reported that the  $\text{NO}_3 + \text{VOC}$  pathway via the  $\text{RONO}_2$  mechanism accounted for 3% of global  $\text{NO}_3^-$  formation on average. The relatively high  $f_{\text{NO}_3+\text{VOC}}$  values observed in Lhasa are broadly consistent with these findings, especially under conditions of high VOC concentrations and strong nighttime oxidant levels.



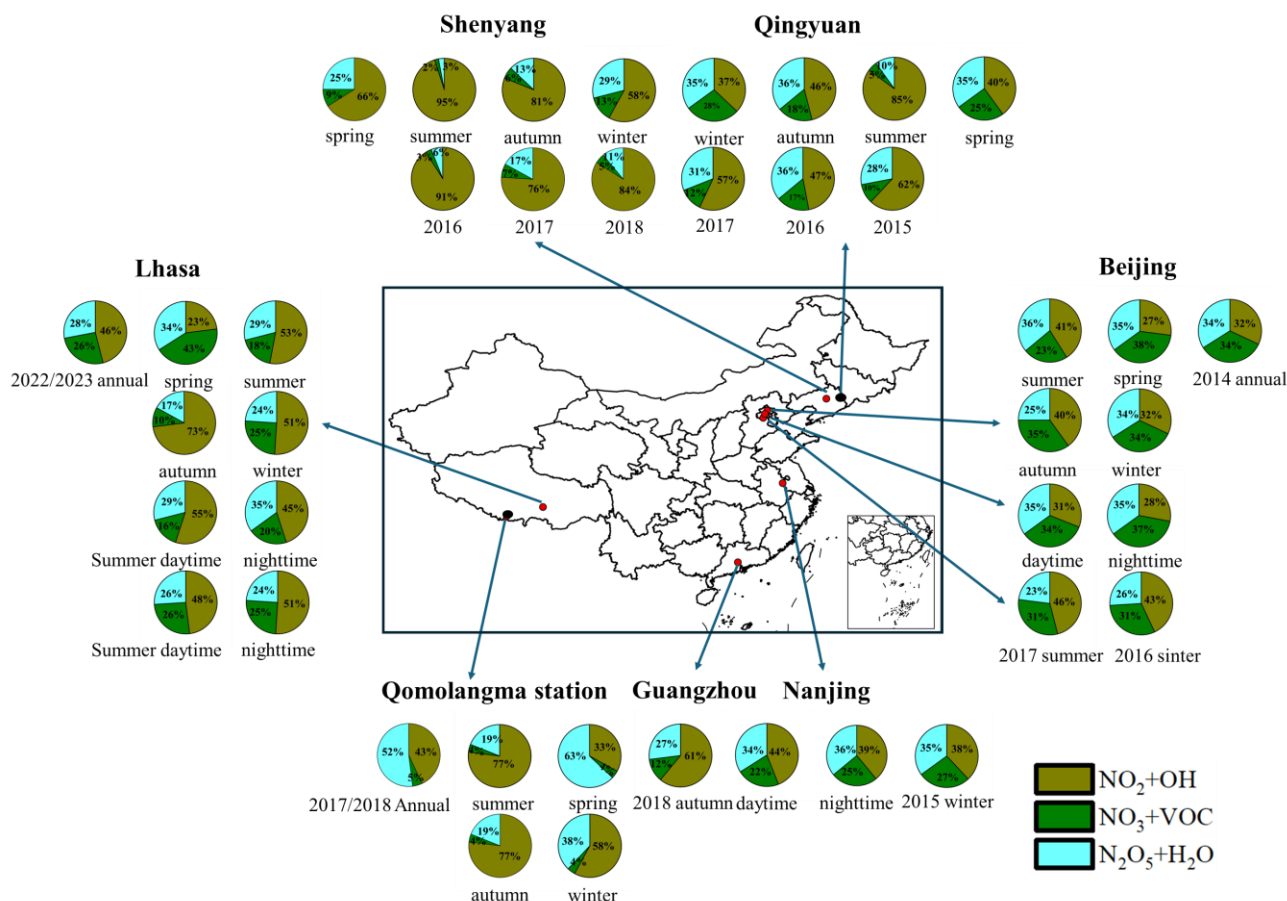


Figure 4. Summary of the relative contributions of key oxidation pathways using the  $\Delta^{17}\text{O}$  methodology around the China (data given in Table S3-S4 in the Supplement). Colors for the study labels indicate the type of sampling location: urban areas (red), and rural/remote areas (black). The pie charts show the relative contribution of different pathways to  $\text{NO}_3^-$  formation:  $f_{\text{NO}_2+\text{OH}}$  (red),  $f_{\text{NO}_3+\text{VOC}}$  (green), and  $f_{\text{N}_2\text{O}_5+\text{H}_2\text{O}}$  (blue).

## 4.2 Seasonal and diurnal variations of $\text{NO}_3^-$ oxidation pathways

Figure S4-S7 illustrates the seasonal variations in the relative contributions of the three main oxidation pathways to  $\text{NO}_3^-$  formation. When comparing different seasons, the  $f_{\text{NO}_2+\text{OH}}$  values were lower ( $p < 0.01$ ) in spring (22.6%) than in winter (50.8%), summer (52.9%) and autumn (73.2%). The dominance of  $\text{NO}_2 + \text{OH}$  pathway in autumn is consistent with observations at Mt. Everest during the autumn seasons of 2017 and 2018, suggesting that  $\text{NO}_3^-$  formation on the Tibetan Plateau in autumn may be mainly driven by  $\text{NO}_2 + \text{OH}$  pathway (Lin et al., 2021; Wang et al., 2020c). The  $\text{NO}_2$  concentration was  $12.7 \pm 1.81 \mu\text{g}/\text{m}^3$  in spring, which was higher than in autumn ( $11.3 \pm 5.83 \mu\text{g}/\text{m}^3$ ). Therefore, the reduced  $f_{\text{NO}_2+\text{OH}}$  in spring cannot be attributed to lower  $\text{NO}_2$  levels. Typically, high solar radiation enhances  $\text{NO}_3^-$  formation via the  $\text{NO}_2 + \text{OH}$  pathway. However, this pathway has been shown

~~to be suppressed in clean atmospheric conditions with low particulate matter loadings (Zhang et al., 2022; Fan et al., 2021). The mean  $\text{NO}_3^-$  concentration was higher in spring ( $0.83 \pm 0.35 \mu\text{g}/\text{m}^3$ ) compared to autumn ( $0.23 \pm 0.13 \mu\text{g}/\text{m}^3$ ), which might account for the higher  $f_{\text{NO}_2+\text{OH}}$  in autumn.~~

A significant increase in the  $f_{\text{NO}_3+\text{VOC}}$  values was observed in spring ( $p < 0.05$ ). First,  $\text{O}_3$  and  $\text{NO}_2$  are precursors of  $\text{NO}_3$ . In this work, ~~highest~~the highest concentrations of  $\text{O}_3$  were found in spring ( $114.9 \pm 18.1 \mu\text{g}/\text{m}^3$ ), likely leading to elevated  $\text{NO}_3$  concentrations. ~~Additionally, The-the~~ low temperature and reduced OH ~~radical~~ concentrations in spring facilitate the reaction of  $\text{NO}_2$  and  $\text{O}_3$  to synthesize  $\text{NO}_3$ . This might be an appropriate reason for the  $f_{\text{NO}_3+\text{VOC}}$  values in spring. High-altitude locations such as Nepal (5079 m a.s.l.) and Qomolangma Station (4300 m a.s.l.) have experienced stratospheric ozone intrusions, especially in spring and winter, as reported in previous studies (Zhang et al., 2025; Cristofanelli et al., 2010; Morin et al., 2007; Zhang et al., 2022; Lin et al., 2016; Yin et al., 2017; Wang et al., 2020c). Notably, such intrusions in spring may elevate tropospheric  $\text{O}_3$  levels in Lhasa, resulting in a mixture of tropospheric and stratospheric  $\text{O}_3$  that enhances  $\text{NO}_3^-$  production. Second, previous study has indicated that the Afghanistan-Pakistan-Tajikistan region, the Indo-Gangetic Plain, and Meghalaya-Myanmar region could transport industrial VOC to various zones in Tibet from west to east. Additionally, agricultural areas in northern India could contribute biomass burning-related VOC to the middle-northern and eastern regions of Tibet (Li et al., 2017). During our sampling campaign, The W and S South and Southeast Asia air clusters were notably prevalent in the springtime, coinciding with intensive fire spots observed in Afghanistan, Pakistan, India, Nepal, and Bhutan (Figure ~~S2S3/S3S4~~). These observations, combined with the prevailing South and Southeast Asia air mass trajectories in spring, strongly suggest that long-range transported VOC from South Asia were delivered to Lhasa and likely participated in local  $\text{NO}_3^-$  production via  $\text{NO}_3 + \text{VOC}$  pathway. Air masses originating from and traversing these regions are likely to pick up VOC emitted from biomass burning and transport them to the sampling site Moreover, recent studies have shown that ambient VOC concentrations in the urban areas on the Qinghai-Tibet Plateau were comparable to those in the North China Plain (Tang et al., 2022). The input of VOC through long-range transport might further elevate VOC concentrations, thereby promoting  $\text{NO}_3^-$  formation via  $\text{NO}_3 + \text{VOC}$  pathway and contributing to the enhanced  $f_{\text{NO}_3+\text{VOC}}$  values observed in spring. While VOC appears to play a dominant role in the process, it should be noted that other nitrogen species (e.g.,  $\text{NO}$ ,  $\text{NO}_2$ ) associated with biomass burning emissions may also be transported over long distances and influence  $\text{NO}_3^-$



formation in Lhasa. These co-transported nitrogen compounds, although not directly quantified in this study, could further contribute to  $\text{NO}_3^-$  production in spring. Taken together, these findings provide strong evidence that long-range transport of biomass burning emissions, particularly from South Asia, can substantially influence springtime  $\text{NO}_3^-$  formation in Lhasa.

Similarly, the  $f_{\text{N}_2\text{O}_5+\text{H}_2\text{O}}$  values exhibited its highest contributions during spring, with significant seasonal differences ( $p < 0.05$ ) except when compared to summer ( $p > 0.05$ ). Typically, high RH enhances  $\text{NO}_3^-$  formation via  $\text{N}_2\text{O}_5 + \text{H}_2\text{O}$  pathway. However, studies have revealed that during sandstorm events, a significant large  $\text{N}_2\text{O}_5$  uptake coefficient is observed on urban aerosols in spring (Xia et al., 2019). In this study, the mean  $\text{Ca}^{2+}$  concentration in  $\text{PM}_{2.5}$  was found to be the highest in spring, suggesting a possible role of dust in facilitating  $\text{N}_2\text{O}_5$  uptake. Additionally,  $\text{N}_2\text{O}_5 + \text{H}_2\text{O}$  pathway has been reported to be promoted by elevated  $\text{NO}_3^-$  concentrations (Lin et al., 2021), which were also highest in spring. Therefore, the increased  $f_{\text{N}_2\text{O}_5+\text{H}_2\text{O}}$  values during spring might be attributed to the combined effects of lower RH, elevated  $\text{Ca}^{2+}$  levels, and high  $\text{NO}_3^-$  concentrations.

Interestingly, distinct diurnal patterns of  $\text{NO}_3^-$  oxidation pathways were observed during the sampling campaign (Figure 5). In summer,  $\text{NO}_2 + \text{OH}$  pathway showed a significantly higher contribution during the daytime (55.1%) compared to nighttime (44.9%), which is attributed to increased OH radical synthesis during longer days and higher temperatures in Lhasa (Rohrer and Berresheim, 2006). A previous study indicated that lower  $\text{NO}_2$  and higher  $\text{O}_3$  concentrations enhance the relative contribution of OH pathway to  $\text{NO}_3^-$  formation (Wang et al., 2019). Additionally, the concentration of ~~aerosol liquid water content~~  $\text{ALWC}$  ( $\text{ALWC}$ , the detailed information is given in Text S3) was higher at night than during the day in summer, favoring  $\text{NO}_3^-$  formation through nocturnal formation. In winter,  $f_{\text{NO}_2+\text{OH}}$ ,  $f_{\text{NO}_3+\text{VOC}}$  and  $f_{\text{N}_2\text{O}_5+\text{H}_2\text{O}}$  were similar during both day and night. Typically, photolytic destruction and chemical reactions with NO are rapid sinks during the daytime, with lifetimes generally less than 5 seconds and resulting in extremely low concentrations. Similarly, the atmospheric lifetime of  $\text{N}_2\text{O}_5$  under sunlight is also very short (Wang et al., 2018). Thus, daytime  $\text{NO}_3$  and  $\text{N}_2\text{O}_5$  chemistry is often considered negligible. However, a recent study revealed that a non-negligible amount of  $\text{NO}_3$  radicals can persist during the daytime in cold months, owing to the limited solar radiation (Hellén et al., 2018). Wang et al. (2020b) found that the daytime production rate of  $\text{NO}_3$  can be substantial due to elevated concentrations of  $\text{O}_3$  and  $\text{NO}_2$ , suggesting that the mixing ratios of  $\text{NO}_3$  and  $\text{N}_2\text{O}_5$  during the day may not be negligible. daytime  $\text{NO}_3$ - and  $\text{N}_2\text{O}_5$ -chemistry is considered

less important due to rapid photolysis of  $\text{NO}_3$  and the titration reaction initiated by  $\text{NO}$ . However, (Wang et al., 2020a) demonstrated that the daytime production rate of  $\text{NO}_3$  can be substantial due to increased concentrations of  $\text{NO}_2$  and  $\text{O}_3$  in winter. Although  $\text{NO}_3$  titration occurs rapidly and the atmospheric lifetimes of  $\text{NO}_3$  and  $\text{N}_2\text{O}_5$  are short, their daytime concentrations are not negligible. A recent study found that in winter, the amount of  $\text{NO}_3$  radical during the day was comparable to that at night, whereas in summer, daytime  $\text{NO}_3$  radicals were lower than those at night (Brown et al., 2011). This discrepancy in  $\text{NO}_3$  radical levels might explain the differences in  $\text{NO}_3^-$  formation pathways between summer and winter. Furthermore, in winter, lower temperatures and elevated  $\text{NO}_2$  concentrations facilitate a quasi-steady-state equilibrium between  $\text{NO}_3$  and  $\text{N}_2\text{O}_5$ , slowing the overall reactivity of the  $\text{NO}_3^-$  precursors (Brown et al., 2003). This equilibrium condition minimizes diurnal fluctuations in precursor concentrations, resulting in relatively stable nocturnal and daytime  $\text{NO}_3^-$  formation pathways, including  $\text{NO}_3 + \text{VOC}$  and  $\text{N}_2\text{O}_5 + \text{H}_2\text{O}$ . Nevertheless, we acknowledge that the exact role of daytime  $\text{NO}_3/\text{N}_2\text{O}_5$  chemistry remains uncertain in Lhasa and should be further assessed using concurrent field observations or chemical transport models. Moreover, when interpreting the diurnal differences in  $\Delta^{17}\text{O}-\text{NO}_3^-$  values, the atmospheric lifetime of  $\text{NO}_3^-$  must be considered. Given the atmospheric lifetime of  $\text{NO}_3^-$  is generally more than 12 hours, each sample might reflect both daytime and nighttime  $\text{NO}_3^-$  production impacting on  $\Delta^{17}\text{O}-\text{NO}_3^-$  values (Park et al., 2004; Vicars et al., 2013).

~~Consequently, under such equilibrium conditions, the  $\text{NO}_2 + \text{OH}$  pathway remains comparatively steady between day and night, as  $\text{OH}$  generation is limited. Conversely, in summer, elevated temperatures and extended photoperiod prevent  $\text{NO}_3$  and  $\text{N}_2\text{O}_5$  from achieving steady state equilibrium, leading to greater variability in  $\text{NO}_3^-$  formation. Thus,  $\text{NO}_3^-$  production becomes more sensitive to photochemical and VOC fluctuations, resulting in a pronounced contrast between daytime and nighttime  $\text{NO}_3^-$  formation pathways (Brown et al., 2003).~~

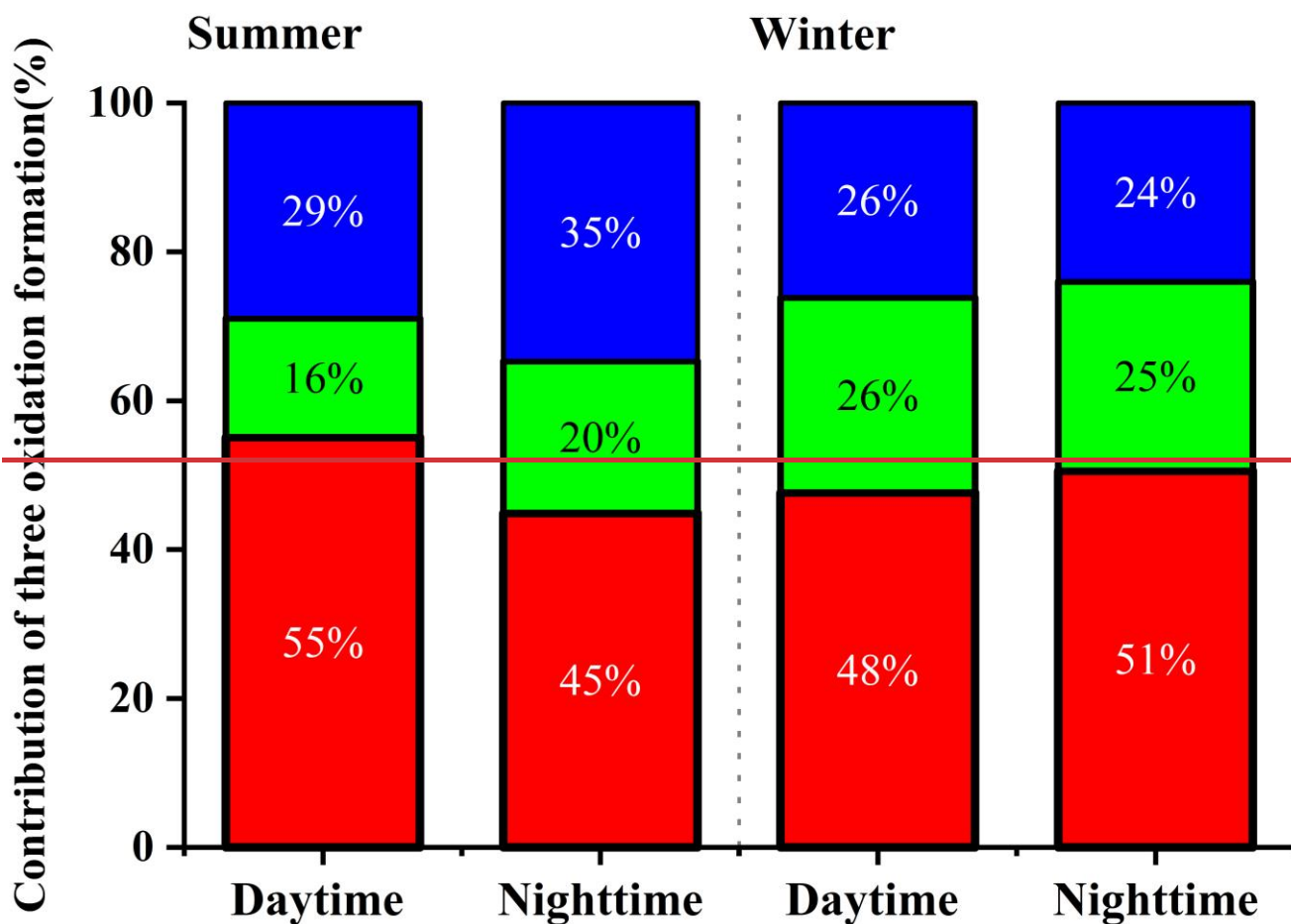


Figure 5. the relative contributions of  $\text{NO}_2+\text{OH}$ ,  $\text{NO}_3+\text{VOC}$ , and  $\text{N}_2\text{O}_5+\text{H}_2\text{O}$  to  $\text{NO}_3^-$  formation during the day and night in summer and winter in Lhasa during the sampling campaign. The contributions are represented as  $f_{\text{NO}_2+\text{OH}}$  (red),  $f_{\text{NO}_3+\text{VOC}}$  (green), and  $f_{\text{N}_2\text{O}_5+\text{H}_2\text{O}}$  (blue).

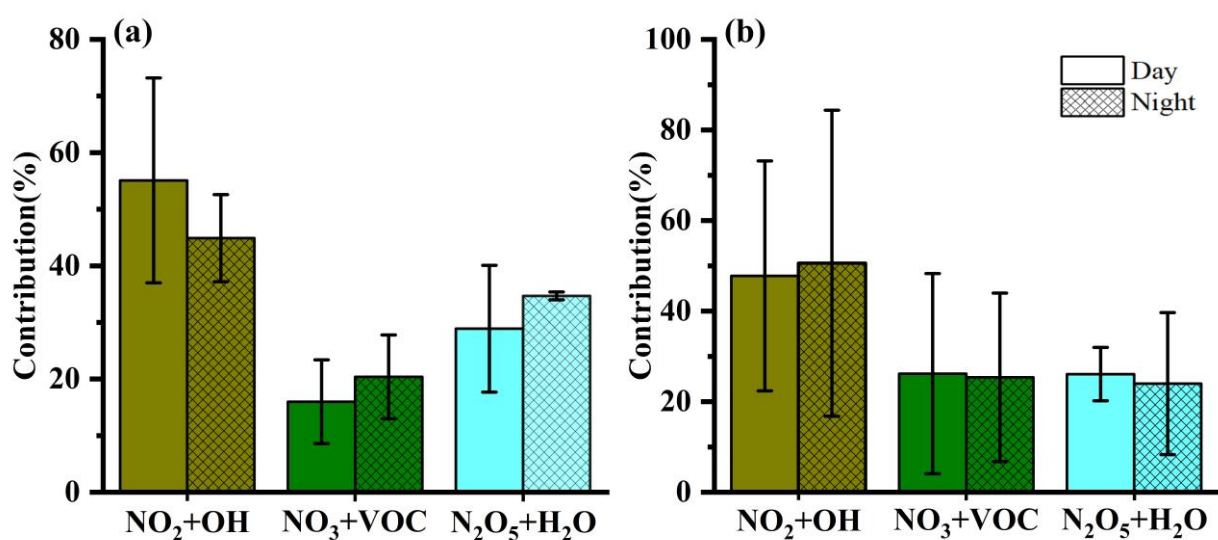
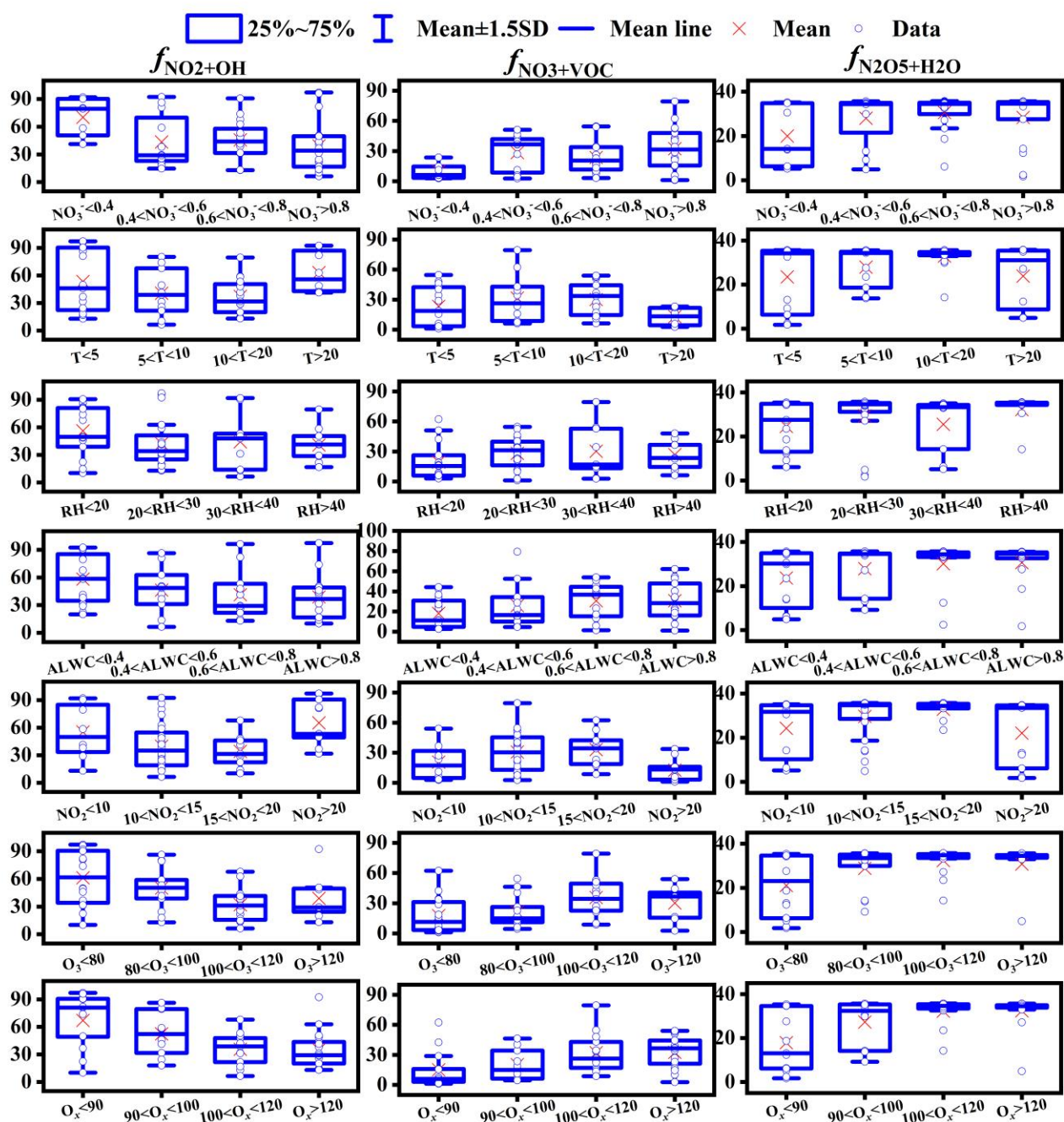


Figure 5. the relative contributions (mean  $\pm$  SD values) of  $\text{NO}_2+\text{OH}$ ,  $\text{NO}_3+\text{VOC}$ , and  $\text{N}_2\text{O}_5+\text{H}_2\text{O}$  to  $\text{NO}_3^-$  formation during the day and night (a) in summer and (b) winter in Lhasa during the sampling campaign.

### 4.3 Integrated analysis of $\text{NO}_3^-$ oxidation pathways in Lhasa

As shown in Figure S4S8,  $\text{NO}_3^- + \text{VOC}$  pathway emerged as the major contributor to  $\text{NO}_3^-$  formation during periods of high  $\text{NO}_3^-$  spikes. To elucidate the  $\text{NO}_3^-$  formation pathways under different  $\text{NO}_3^-$  concentrations,  $\text{NO}_3^-$  samples were categorized into different concentration ranges~~To elucidate the mechanisms driving  $\text{NO}_3^-$  formation under varying conditions,  $\text{NO}_3^-$  samples were categorized into different concentration ranges~~ (Figure 6). We found the  $f_{\text{NO}_3+\text{VOC}}$  values increased and  $f_{\text{NO}_2+\text{OH}}$  values decreased with the  $\text{NO}_3^-$  concentrations. Although recent field radical measurements in urban sites in China found that OH and  $\text{HO}_2$  radical during haze period is comparable to clean days (Slater et al., 2020; Yang et al., 2021), our results suggested that  $\text{NO}_3+\text{VOC}$  pathway still played an important role in  $\text{NO}_3^-$  production under high- $\text{NO}_3^-$  concentration in Lhasa, possibly due to enhanced VOC emission. This significant decrease in  $f_{\text{NO}_2+\text{OH}}$  values in the air pollution is predictable, as OH radical production tends to decline with increasing air pollution, especially on heavily polluted and hazy days (Bäumer et al., 2008). In addition to concentration effects, meteorological factors typically also regulate the  $\text{NO}_3^-$  oxidation pathways. Typically, high temperature promotes the  $\text{NO}_3^-$  formation in  $f_{\text{NO}_2+\text{OH}}$  values (Han et al., 2015). However, our study revealed that the relationship between temperature and  $f_{\text{NO}_2+\text{OH}}$  values did not consistently show a positive trend. Further analysis indicated that  $\text{NO}_2$  and  $\text{O}_3$  concentrations were negatively correlated, with lower  $\text{NO}_2$  concentrations paired with elevated  $\text{O}_3$  levels (Figure S5S9).  $f_{\text{NO}_2+\text{OH}}$  values reached its minimum when  $\text{NO}_2$  was between 15 and 20  $\mu\text{g}/\text{m}^3$  and  $\text{O}_3$  was within 100-120  $\mu\text{g}/\text{m}^3$ . Although OH radicals exhibit a higher oxidation potential (2.8 V) than  $\text{O}_3$  (2.07 V), but atmospheric availability is much lower than that of  $\text{O}_3$  (Carslaw et al., 1999; Dubey et al., 1997). Therefore,  $\text{NO}_2$  at lower concentrations is more likely to be oxidized by OH than by  $\text{O}_3$ , even though  $\text{O}_3$  concentrations were high. With increasing  $\text{NO}_2$  concentrations, the availability of OH radicals for oxidating  $\text{NO}_2$  became lower, resulting in a relatively higher proportion of  $\text{NO}_2$  being oxidized by  $\text{O}_3$  although  $\text{O}_3$  concentrations were low. However, when the concentration of  $\text{O}_3$  is below 20  $\mu\text{g}/\text{m}^3$ ,  $\text{O}_3$  concentrations were not sufficient to oxidize  $\text{NO}_2$  due to the higher  $\text{NO}_2$  concentrations and OH radicals for oxidating  $\text{NO}_2$  would re-dominate. These observations underscore that in high-altitude urban environments like Lhasa, OH effectiveness is more important on  $\text{NO}_3^-$  oxidation pathways than that of  $\text{O}_3$ . Additionally, we identified an intriguing positive correlation between the atmospheric oxidizing capacity ( $\text{O}_x = \text{NO}_2 + \text{O}_3$ ) and  $f_{\text{NO}_3+\text{VOC}}$  values.  $f_{\text{NO}_3+\text{VOC}}$  values were lowest when  $\text{O}_x$  was less than 90  $\mu\text{g}/\text{m}^3$ , corresponding to a maximum contribution from the  $\text{NO}_2$

531 + OH pathway. This suggests that  $O_x$  is more indicative of the pathways of  $NO_3^-$  formation in the  
 532 atmosphere compared to either  $NO_2$  or  $O_3$  alone. Typically, High RH and ALWC were also positively  
 533 correlated with  $f_{N_2O_5+H_2O}$ . But RH was associated with variable contributions from the  $N_2O_5+H_2O$   
 534 pathway in our study, while increasing ALWC significantly enhanced this pathway, indicating ALWC  
 535 as a more reliable indicator of  $NO_3^-$  formation.



536  
 537 Figure 6 Influence of  $NO_3^-$  ( $\mu g/m^3$ ), temperature ( $^{\circ}C$ ), RH (%), ALWC ( $\mu g/m^3$ ),  $NO_2$  ( $\mu g/m^3$ ),  $O_3$  and  
 538  $O_x$  ( $\mu g/m^3$ ) on  $NO_3^-$  formation pathways (%).

#### 539 4.4 Implications



The oxidation pathways of  $\text{NO}_3^-$  in Lhasa, China, were constrained using a full year of  $\Delta^{17}\text{O}-\text{NO}_3^-$  measurements from 2022 to 2023. Based on seasonal data, we observed a significant increase in the relative contribution of the  $\text{NO}_3+\text{VOC}$  to  $\text{NO}_3^-$  formation during ~~the~~ spring. Furthermore, the diurnal distribution of  $\text{NO}_3^-$  oxidation pathways varied distinctly across seasons. To better understand the factors influencing these pathways, we integrated meteorological conditions,  $\text{NO}_x$  precursors, and ALWC for a more comprehensive analysis of  $\text{NO}_3^-$  formation. The results revealed that  $\text{O}_x$  and ALWC are more reliable indicators of  $\text{NO}_3^-$  oxidation pathways than meteorological factors. Notably, Lhasa's unique high-altitude environment such as strong solar radiation, persistently high  $\text{O}_3$ , and elevated VOC, promotes active  $\text{NO}_3 + \text{VOC}$  chemistry, especially in spring. Atmospheric ALWC is primarily produced by hygroscopic aerosols such as  $\text{SO}_4^{2-}$ ,  $\text{NH}_4^+$ , and  $\text{Cl}^-$ . Therefore, in addition to controlling  $\text{NO}_2$ ,  $\text{O}_3$ , and VOC, reducing these hygroscopic aerosols is crucial for effective  $\text{PM}_{2.5}$  pollution control.

Although this study provides valuable insights into  $\text{NO}_3^-$  formation mechanisms in Lhasa, we must acknowledge the associated uncertainties due to the lack of comprehensive observational constraints in Lhasa. Specifically, the limited understanding of local  $\text{RO}_2$  concentrations led us to adopt empirical parameterizations and refer to measurements from other regions, which inevitably introduce uncertainty into the pathway apportionment. In addition, the absence of direct observations of nighttime  $\text{NO}$  emissions and the  $\text{NO}_2$ - $\text{NO}$  isotope exchange processes in this region further complicates the interpretation of diurnal variations in  $\text{NO}_3^-$  formation pathways. To improve the robustness of  $\Delta^{17}\text{O}$ -based pathway analysis, future studies should consider synchronous measurements of both  $\text{NO}_2$  and  $\text{NO}_3^-$  isotopes.

## Data availability

All data are presented in the main text and/ or the Supplement. For additional data, please contact the corresponding author ([liu.junwen@jnu.edu.cn](mailto:liu.junwen@jnu.edu.cn)).

## Author contributors

JL designed, conceived, and led the research. XZ performed the data analysis and drafted the manuscript. JL, XZ NC and BB planned and carried out the measurements. NC, BB and PD were responsible for measuring the meteorological parameters. JL and PY secured funding for the continuous aerosol sampling and analysis. FC and YZ provided expertise on isotope analysis methods. JL offered guidance on data analysis, and all authors contributed to revising the manuscript.



570 **Competing interests**

571 The authors declare no competing financial interest.

572 **Acknowledgments**

573 This study was supported by the Natural Science Foundation of Xizang Autonomous Region  
574 (XZ202401ZR0067), Guangdong Basic and Applied Basic Research Foundation (2024B1515040026),  
575 ~~and~~ the second Tibetan Plateau Scientific Expedition and Research Program (20190ZKK0604) and  
576 Guangdong Provincial General Colleges and Universities Innovation Team Project (Natural Science)  
577 (2024KCXTD004).

578

## Reference

- Alexander, B., Hastings, M., Allman, D., Dachs, J., Thornton, J., and Kunasek, S.: Quantifying atmospheric nitrate formation pathways based on a global model of the oxygen isotopic composition ( $\Delta^{17}\text{O}$ ) of atmospheric nitrate, *Atmospheric Chemistry and Physics*, 9, 5043-5056, 2009.
- Alexander, B., Sherwen, T., Holmes, C. D., Fisher, J. A., Chen, Q., Evans, M. J., and Kasibhatla, P.: Global inorganic nitrate production mechanisms: comparison of a global model with nitrate isotope observations, *Atmospheric Chemistry and Physics*, 20, 3859-3877, 2020.
- Barkan, E. and Luz, B.: High-precision measurements of  $^{17}\text{O}/^{16}\text{O}$  and  $^{18}\text{O}/^{16}\text{O}$  of  $\text{O}_2$  and  $\text{O}_2/\text{Ar}$  ratio in air, *Rapid communications in mass spectrometry*, 17, 2809-2814, 2003.
- Bäumer, D., Vogel, B., Versick, S., Rinke, R., Möhler, O., and Schnaiter, M.: Relationship of visibility, aerosol optical thickness and aerosol size distribution in an ageing air mass over South-West Germany, *Atmospheric Environment*, 42, 989-998, 2008.
- Bell, M. L., Dominici, F., Ebisu, K., Zeger, S. L., and Samet, J. M.: Spatial and temporal variation in  $\text{PM}_{2.5}$  chemical composition in the United States for health effects studies, *Environmental health perspectives*, 115, 989-995, 2007.
- Brown, S. S. and Stutz, J.: Nighttime radical observations and chemistry, *Chemical Society Reviews*, 41, 6405-6447, 2012.
- Brown, S. S., Stark, H., and Ravishankara, A.: Applicability of the steady state approximation to the interpretation of atmospheric observations of  $\text{NO}_3$  and  $\text{N}_2\text{O}_5$ , *Journal of Geophysical Research: Atmospheres*, 108, 2003.
- Brown, S. S., Dubé, W. P., Peischl, J., Ryerson, T. B., Atlas, E., Warneke, C., de Gouw, J. A., te Lintel Hekkert, S., Brock, C. A., and Flocke, F.: Budgets for nocturnal VOC oxidation by nitrate radicals aloft during the 2006 Texas Air Quality Study, *Journal of Geophysical Research: Atmospheres*, 116, 2011.
- Cao, X., Xing, Q., Hu, S., Xu, W., Xie, R., Xian, A., Xie, W., Yang, Z., and Wu, X.: Characterization, reactivity, source apportionment, and potential source areas of ambient volatile organic compounds in a typical tropical city, *Journal of Environmental Sciences*, 123, 417-429, 2023.
- Carslaw, N., Creasey, D. J., Heard, D. E., Lewis, A. C., McQuaid, J. B., Pilling, M. J., Monks, P. S., Bandy, B. J., and Penkett, S. A.: Modeling OH,  $\text{HO}_2$ , and  $\text{RO}_2$  radicals in the marine boundary layer: 1. Model construction and comparison with field measurements, *Journal of Geophysical Research:*

609 Atmospheres, 104, 30241-30255, <https://doi.org/10.1029/1999JD900783>, 1999.

610 Chen, Z., Pei, C., Liu, J., Zhang, X., Ding, P., Dang, L., Zong, Z., Jiang, F., Wu, L., and Sun, X.: Non-  
611 agricultural source dominates the ammonium aerosol in the largest city of South China based on the  
612 vertical  $\delta^{15}\text{N}$  measurements, *Science of The Total Environment*, 848, 157750, 2022.

613 Clark, C. M. and Tilman, D.: Loss of plant species after chronic low-level nitrogen deposition to prairie  
614 grasslands, *Nature*, 451, 712-715, 2008.

615 Colmer, J., Hardman, I., Shimshack, J., and Voorheis, J.: Disparities in  $\text{PM}_{2.5}$  air pollution in the United  
616 States, *Science*, 369, 575-578, 2020.

617 Cristofanelli, P., Bracci, A., Sprenger, M., Marinoni, A., Bonafè, U., Calzolari, F., Duchi, R., Laj, P.,  
618 Pichon, J.-M., and Roccato, F.: Tropospheric ozone variations at the Nepal Climate Observatory-  
619 Pyramid (Himalayas, 5079 m asl) and influence of deep stratospheric intrusion events, *Atmospheric*  
620 *Chemistry and Physics*, 10, 6537-6549, 2010.

621 Daily, B., <https://xinwen.bjd.com.cn/content/s6340d130e4b0b60bbc5d4ecd.html>

622 Dubey, M. K., Mohrschladt, R., Donahue, N. M., and Anderson, J. G.: Isotope specific kinetics of  
623 hydroxyl radical (OH) with water ( $\text{H}_2\text{O}$ ): Testing models of reactivity and atmospheric fractionation,  
624 *The Journal of Physical Chemistry A*, 101, 1494-1500, 1997.

625 Espina-Martin, P., Perdrix, E., Alleman, L., and Coddeville, P.: Origins of the seasonal variability of  
626  $\text{PM}_{2.5}$  sources in a rural site in Northern France, *Atmospheric Environment*, 120660, 2024.

627 Fan, M.-Y., Zhang, Y.-L., Lin, Y.-C., Hong, Y., Zhao, Z.-Y., Xie, F., Du, W., Cao, F., Sun, Y., and Fu,  
628 P.: Important role of  $\text{NO}_3$  radical to nitrate formation aloft in urban Beijing: Insights from triple  
629 oxygen isotopes measured at the tower, *Environmental Science & Technology*, 56, 6870-6879, 2021.

630 Feng, X., Chen, Y., Chen, S., Peng, Y., Liu, Z., Jiang, M., Feng, Y., Wang, L., Li, L., and Chen, J.:  
631 Dominant Contribution of  $\text{NO}_3$  Radical to  $\text{NO}_3^-$  Formation during Heavy Haze Episodes: Insights  
632 from High-Time Resolution of Dual Isotopes  $\Delta^{17}\text{O}$  and  $\delta^{18}\text{O}$ , *Environmental Science &*  
633 *Technology*, 57, 20726-20735, 2023.

634 Fisher, J. A., Jacob, D. J., Travis, K. R., Kim, P. S., Marais, E. A., Chan Miller, C., Yu, K., Zhu, L.,  
635 Yantosca, R. M., Sulprizio, M. P., Mao, J., Wennberg, P. O., Crounse, J. D., Teng, A. P., Nguyen, T.  
636 B., St. Clair, J. M., Cohen, R. C., Romer, P., Nault, B. A., Wooldridge, P. J., Jimenez, J. L.,  
637 Campuzano-Jost, P., Day, D. A., Hu, W., Shepson, P. B., Xiong, F., Blake, D. R., Goldstein, A. H.,  
638 Misztal, P. K., Hanisco, T. F., Wolfe, G. M., Ryerson, T. B., Wisthaler, A., and Mikoviny, T.: Organic

639 nitrate chemistry and its implications for nitrogen budgets in an isoprene- and monoterpene-rich  
640 atmosphere: constraints from aircraft (SEAC4RS) and ground-based (SOAS) observations in the  
641 Southeast US, *Atmos. Chem. Phys.*, 16, 5969-5991, 10.5194/acp-16-5969-2016, 2016.

642 Ge, S., Su, J., Zhao, P., Li, J., Liu, S., Qiu, Y., Pu, W., and Ma, Z.: Characteristics of PM<sub>2.5</sub>  
643 hygroscopicity and the influences of water-soluble ions during haze events in Beijing, *Atmospheric*  
644 *Environment*, 322, 120382, <https://doi.org/10.1016/j.atmosenv.2024.120382>, 2024.

645 Geng, G., Zheng, Y., Zhang, Q., Xue, T., Zhao, H., Tong, D., Zheng, B., Li, M., Liu, F., and Hong, C.:  
646 Drivers of PM<sub>2.5</sub> air pollution deaths in China 2002–2017, *Nature Geoscience*, 14, 645-650, 2021.

647 Han, T., Liu, X., Zhang, Y., Qu, Y., Zeng, L., Hu, M., and Zhu, T.: Role of secondary aerosols in haze  
648 formation in summer in the Megacity Beijing, *Journal of environmental sciences*, 31, 51-60, 2015.

649 He, P., Xie, Z., Chi, X., Yu, X., Fan, S., Kang, H., Liu, C., and Zhan, H.: Atmospheric  $\Delta^{17}\text{O}(\text{NO}_3^-)$   
650 reveals nocturnal chemistry dominates nitrate production in Beijing haze, *Atmospheric Chemistry*  
651 *and Physics*, 18, 14465-14476, 2018.

652 He, S., Huang, M., Zheng, L., Chang, M., Chen, W., Xie, Q., and Wang, X.: Seasonal variation of  
653 transport pathways and potential source areas at high inorganic nitrogen wet deposition sites in  
654 southern China, *Journal of Environmental Sciences*, 114, 444-453,  
655 <https://doi.org/10.1016/j.jes.2021.12.024>, 2022.

656 Hellén, H., Praplan, A. P., Tykkä, T., Ylivinkka, I., Vakkari, V., Bäck, J., Petäjä, T., Kulmala, M., and  
657 Hakola, H.: Long-term measurements of volatile organic compounds highlight the importance of  
658 sesquiterpenes for the atmospheric chemistry of a boreal forest, *Atmospheric Chemistry and Physics*,  
659 18, 13839-13863, 2018.

660 Huang, R.-J., Zhang, Y., Bozzetti, C., Ho, K.-F., Cao, J.-J., Han, Y., Daellenbach, K. R., Slowik, J. G.,  
661 Platt, S. M., and Canonaco, F.: High secondary aerosol contribution to particulate pollution during  
662 haze events in China, *Nature*, 514, 218-222, 2014.

663 Ishino, S., Hattori, S., Savarino, J., Jourdain, B., Preunkert, S., Legrand, M., Caillon, N., Barbero, A.,  
664 Kuribayashi, K., and Yoshida, N.: Seasonal variations of triple oxygen isotopic compositions of  
665 atmospheric sulfate, nitrate, and ozone at Dumont d'Urville, coastal Antarctica, *Atmospheric*  
666 *Chemistry and Physics*, 17, 3713-3727, 2017.

667 Kanaya, Y., Cao, R., Akimoto, H., Fukuda, M., Komazaki, Y., Yokouchi, Y., Koike, M., Tanimoto, H.,  
668 Takegawa, N., and Kondo, Y.: Urban photochemistry in central Tokyo: 1. Observed and modeled

669 OH and HO<sub>2</sub> radical concentrations during the winter and summer of 2004, Journal of Geophysical  
670 Research: Atmospheres, 112, 2007.

671 Kunasek, S., Alexander, B., Steig, E., Hastings, M., Gleason, D., and Jarvis, J.: Measurements and  
672 modeling of  $\Delta^{17}\text{O}$  of nitrate in snowpits from Summit, Greenland, Journal of Geophysical Research:  
673 Atmospheres, 113, 2008.

674 Lhasa, T. P. s. G. o., Overview of Lhasa: <https://www.lasa.gov.cn/lasa/yxls/yx.shtml>

675 Li, H., He, Q., Song, Q., Chen, L., Song, Y., Wang, Y., Lin, K., Xu, Z., and Shao, M.: Diagnosing  
676 Tibetan pollutant sources via volatile organic compound observations, Atmospheric Environment,  
677 166, 244-254, 2017.

678 Li, Z., Walters, W. W., Hastings, M. G., Song, L., Huang, S., Zhu, F., Liu, D., Shi, G., Li, Y., and Fang,  
679 Y.: Atmospheric nitrate formation pathways in urban and rural atmosphere of Northeast China:  
680 Implications for complicated anthropogenic effects, Environmental Pollution, 296, 118752,  
681 <https://doi.org/10.1016/j.envpol.2021.118752>, 2022.

682 Lin, M., Zhang, Z., Su, L., Hill-Falkenthal, J., Priyadarshi, A., Zhang, Q., Zhang, G., Kang, S., Chan,  
683 C. Y., and Thiemens, M. H.: Resolving the impact of stratosphere-to-troposphere transport on the  
684 sulfur cycle and surface ozone over the Tibetan Plateau using a cosmogenic <sup>35</sup>S tracer, Journal of  
685 Geophysical Research: Atmospheres, 121, 439-456, 2016.

686 Lin, Y.-C., Zhang, Y.-L., Yu, M., Fan, M.-Y., Xie, F., Zhang, W.-Q., Wu, G., Cong, Z., and Michalski,  
687 G.: Formation mechanisms and source apportionments of airborne nitrate aerosols at a Himalayan-  
688 Tibetan Plateau site: Insights from nitrogen and oxygen isotopic compositions, Environmental  
689 Science & Technology, 55, 12261-12271, 2021.

690 Luo, L., Kao, S., Wu, Y., Zhang, X., Lin, H., Zhang, R., and Xiao, H.: Stable oxygen isotope constraints  
691 on nitrate formation in Beijing in springtime, Environmental Pollution, 263, 114515, 2020.

692 Michalski, G., Scott, Z., Kabling, M., and Thiemens, M. H.: First measurements and modeling of  
693  $\Delta^{17}\text{O}$  in atmospheric nitrate, Geophysical Research Letters, 30, 2003.

694 Morin, S., Savarino, J., Bekki, S., Gong, S., and Bottenheim, J.: Signature of Arctic surface ozone  
695 depletion events in the isotope anomaly ( $\Delta^{17}\text{O}$ ) of atmospheric nitrate, Atmospheric Chemistry and  
696 Physics, 7, 1451-1469, 2007.

697 Park, R. J., Jacob, D. J., Field, B. D., Yantosca, R. M., and Chin, M.: Natural and transboundary  
698 pollution influences on sulfate-nitrate-ammonium aerosols in the United States: Implications for

699 policy, *Journal of Geophysical Research: Atmospheres*, 109, 2004.

700 Parnell, A. C., Inger, R., Bearhop, S., and Jackson, A. L.: Source partitioning using stable isotopes:  
 701 coping with too much variation, *PloS one*, 5, e9672, 2010.

702 Qiu, X., Ying, Q., Wang, S., Duan, L., Zhao, J., Xing, J., Ding, D., Sun, Y., Liu, B., Shi, A., Yan, X.,  
 703 Xu, Q., and Hao, J.: Modeling the impact of heterogeneous reactions of chlorine on summertime  
 704 nitrate formation in Beijing, China, *Atmos. Chem. Phys.*, 19, 6737-6747, 10.5194/acp-19-6737-  
 705 2019, 2019.

706 Rohrer, F. and Berresheim, H.: Strong correlation between levels of tropospheric hydroxyl radicals and  
 707 solar ultraviolet radiation, *Nature*, 442, 184-187, 2006.

708 Salameh, D., Detournay, A., Pey, J., Pérez, N., Liguori, F., Saraga, D., Bove, M. C., Brotto, P., Cassola,  
 709 F., and Massabò, D.: PM<sub>2.5</sub> chemical composition in five European Mediterranean cities: A 1-year  
 710 study, *Atmospheric Research*, 155, 102-117, 2015.

711 Savarino, J., Vicars, W. C., Legrand, M., Preunkert, S., Jourdain, B., Frey, M. M., Kukui, A., Caillon,  
 712 N., and Gil Roca, J.: Oxygen isotope mass balance of atmospheric nitrate at Dome C, East Antarctica,  
 713 during the OPALE campaign, *Atmospheric Chemistry and Physics*, 16, 2659-2673, 2016.

714 Slater, E. J., Whalley, L. K., Woodward-Massey, R., Ye, C., Lee, J. D., Squires, F., Hopkins, J. R.,  
 715 Dunmore, R. E., Shaw, M., Hamilton, J. F., Lewis, A. C., Crilley, L. R., Kramer, L., Bloss, W., Vu,  
 716 T., Sun, Y., Xu, W., Yue, S., Ren, L., Acton, W. J. F., Hewitt, C. N., Wang, X., Fu, P., and Heard, D.  
 717 E.: Elevated levels of OH observed in haze events during wintertime in central Beijing, *Atmos.*  
 718 *Chem. Phys.*, 20, 14847-14871, 10.5194/acp-20-14847-2020, 2020.

719 Song, W., Wang, Y.-L., Yang, W., Sun, X.-C., Tong, Y.-D., Wang, X.-M., Liu, C.-Q., Bai, Z.-P., and  
 720 Liu, X.-Y.: Isotopic evaluation on relative contributions of major NO<sub>x</sub> sources to nitrate of PM<sub>2.5</sub> in  
 721 Beijing, *Environmental Pollution*, 248, 183-190, 2019.

722 Su, X., Tie, X., Li, G., Cao, J., Huang, R., Feng, T., Long, X., and Xu, R.: Effect of hydrolysis of N<sub>2</sub>O<sub>5</sub>  
 723 on nitrate and ammonium formation in Beijing China: WRF-Chem model simulation, *Science of*  
 724 *The Total Environment*, 579, 221-229, <https://doi.org/10.1016/j.scitotenv.2016.11.125>, 2017.

725 Sun, P., Farley, R. N., Li, L., Srivastava, D., Niedek, C. R., Li, J., Wang, N., Cappa, C. D., Pusede, S.  
 726 E., and Yu, Z.: PM<sub>2.5</sub> composition and sources in the San Joaquin Valley of California: A long-term  
 727 study using ToF-ACSM with the capture vaporizer, *Environmental Pollution*, 292, 118254, 2022.

728 Tang, G., Yao, D., Kang, Y., Liu, Y., Liu, Y., Wang, Y., Bai, Z., Sun, J., Cong, Z., Xin, J., Liu, Z., Zhu,



729 Z., Geng, Y., Wang, L., Li, T., Li, X., Bian, J., and Wang, Y.: The urgent need to control volatile  
 730 organic compound pollution over the Qinghai-Tibet Plateau, *iScience*, 25, 105688,  
 731 <https://doi.org/10.1016/j.isci.2022.105688>, 2022.

732 Vicars, W., Morin, S., Savarino, J., Wagner, N., Erbland, J., Vince, E., Martins, J., Lerner, B., Quinn,  
 733 P., and Coffman, D.: Spatial and diurnal variability in reactive nitrogen oxide chemistry as reflected  
 734 in the isotopic composition of atmospheric nitrate: Results from the CalNex 2010 field study, *Journal*  
 735 *of Geophysical Research: Atmospheres*, 118, 10,567-510,588, 2013.

736 Vicars, W. C. and Savarino, J.: Quantitative constraints on the  $^{17}\text{O}$ -excess ( $\Delta^{17}\text{O}$ ) signature of surface  
 737 ozone: Ambient measurements from 50 N to 50 S using the nitrite-coated filter technique,  
 738 *Geochimica et Cosmochimica Acta*, 135, 270-287, 2014.

739 Vicars, W. C., Bhattacharya, S., Erbland, J., and Savarino, J.: Measurement of the  $^{17}\text{O}$ -excess ( $\Delta^{17}\text{O}$ )  
 740 of tropospheric ozone using a nitrite-coated filter, *Rapid Communications in Mass Spectrometry*,  
 741 26, 1219-1231, 2012.

742 Walters, W. W., Pye, H. O., Kim, H., and Hastings, M. G.: Modeling the Oxygen Isotope Anomaly  
 743 ( $\Delta^{17}\text{O}$ ) of Reactive Nitrogen in the Community Multiscale Air Quality Model: Insights into Nitrogen  
 744 Oxide Chemistry in the Northeastern United States, *ACS ES&T Air*, 2024.

745 Wang, H., Chen, X., Lu, K., Hu, R., Li, Z., Wang, H., Ma, X., Yang, X., Chen, S., and Dong, H.:  $\text{NO}_3$   
 746 and  $\text{N}_2\text{O}_5$  chemistry at a suburban site during the EXPLORE-YRD campaign in 2018, *Atmospheric*  
 747 *Environment*, 224, 117180, 2020a.

748 Wang, H., Chen, X., Lu, K., Hu, R., Li, Z., Wang, H., Ma, X., Yang, X., Chen, S., Dong, H., Liu, Y.,  
 749 Fang, X., Zeng, L., Hu, M., and Zhang, Y.:  $\text{NO}_3$  and  $\text{N}_2\text{O}_5$  chemistry at a suburban site during the  
 750 EXPLORE-YRD campaign in 2018, *Atmospheric Environment*, 224, 117180,  
 751 <https://doi.org/10.1016/j.atmosenv.2019.117180>, 2020b.

752 Wang, H., Lu, K., Guo, S., Wu, Z., Shang, D., Tan, Z., Wang, Y., Le Breton, M., Lou, S., Tang, M.,  
 753 Wu, Y., Zhu, W., Zheng, J., Zeng, L., Hallquist, M., Hu, M., and Zhang, Y.: Efficient  $\text{N}_2\text{O}_5$  uptake  
 754 and  $\text{NO}_3$  oxidation in the outflow of urban Beijing, *Atmos. Chem. Phys.*, 18, 9705-9721,  
 755 10.5194/acp-18-9705-2018, 2018.

756 Wang, K., Hattori, S., Kang, S., Lin, M., and Yoshida, N.: Isotopic constraints on the formation  
 757 pathways and sources of atmospheric nitrate in the Mt. Everest region, *Environmental Pollution*,  
 758 267, 115274, 2020c.

759 Wang, Y., Liu, J., Jiang, F., Chen, Z., Wu, L., Zhou, S., Pei, C., Kuang, Y., Cao, F., and Zhang, Y.:  
760 Vertical measurements of stable nitrogen and oxygen isotope composition of fine particulate nitrate  
761 aerosol in Guangzhou city: Source apportionment and oxidation pathway, *Science of The Total*  
762 *Environment*, 865, 161239, 2023.

763 Wang, Y. L., Song, W., Yang, W., Sun, X. C., Tong, Y. D., Wang, X. M., Liu, C. Q., Bai, Z. P., and Liu,  
764 X. Y.: Influences of atmospheric pollution on the contributions of major oxidation pathways to PM<sub>2.5</sub>  
765 nitrate formation in Beijing, *Journal of Geophysical Research: Atmospheres*, 124, 4174-4185,  
766 2019.

767 Xia, M., Wang, W., Wang, Z., Gao, J., Li, H., Liang, Y., Yu, C., Zhang, Y., Wang, P., Zhang, Y., Bi, F.,  
768 Cheng, X., and Wang, T.: Heterogeneous Uptake of N<sub>2</sub>O<sub>5</sub> in Sand Dust and Urban Aerosols  
769 Observed during the Dry Season in Beijing, *Atmosphere*, 10, 204, 2019.

770 Xu, Q., Wang, S., Jiang, J., Bhattarai, N., Li, X., Chang, X., Qiu, X., Zheng, M., Hua, Y., and Hao, J.:  
771 Nitrate dominates the chemical composition of PM<sub>2.5</sub> during haze event in Beijing, China, *Science*  
772 *of the Total Environment*, 689, 1293-1303, 2019.

773 Yang, X., Lu, K., Ma, X., Liu, Y., Wang, H., Hu, R., Li, X., Lou, S., Chen, S., and Dong, H.:  
774 Observations and modeling of OH and HO<sub>2</sub> radicals in Chengdu, China in summer 2019, *Science*  
775 *of The Total Environment*, 772, 144829, 2021.

776 Yin, M., Guan, H., Luo, L., Xiao, H., and Zhang, Z.: Using nitrogen and oxygen stable isotopes to  
777 analyze the major NO<sub>x</sub> sources to nitrate of PM<sub>2.5</sub> in Lanzhou, northwest China, in winter-spring  
778 periods, *Atmospheric Environment*, 276, 119036, 2022.

779 Yin, X., Kang, S., de Foy, B., Cong, Z., Luo, J., Zhang, L., Ma, Y., Zhang, G., Rupakheti, D., and  
780 Zhang, Q.: Surface ozone at Nam Co in the inland Tibetan Plateau: variation, synthesis comparison  
781 and regional representativeness, *Atmospheric Chemistry and Physics*, 17, 11293-11311, 2017.

782 Zhang, Q., Zheng, Y., Tong, D., Shao, M., Wang, S., Zhang, Y., Xu, X., Wang, J., He, H., and Liu, W.:  
783 Drivers of improved PM<sub>2.5</sub> air quality in China from 2013 to 2017, *Proceedings of the National*  
784 *Academy of Sciences*, 116, 24463-24469, 2019.

785 Zhang, Q., Jiang, X., Tong, D., Davis, S. J., Zhao, H., Geng, G., Feng, T., Zheng, B., Lu, Z., Streets,  
786 D. G., Ni, R., Brauer, M., van Donkelaar, A., Martin, R. V., Huo, H., Liu, Z., Pan, D., Kan, H., Yan,  
787 Y., Lin, J., He, K., and Guan, D.: Transboundary health impacts of transported global air pollution  
788 and international trade, *Nature*, 543, 705-709, 10.1038/nature21712, 2017.

789 Zhang, Y.-L., Zhang, W., Fan, M.-Y., Li, J., Fang, H., Cao, F., Lin, Y.-C., Wilkins, B. P., Liu, X., and  
790 Bao, M.: A diurnal story of  $\Delta^{17}\text{O}(\text{NO}_3^-)$  in urban Nanjing and its implication for nitrate aerosol  
791 formation, *npj Climate and Atmospheric Science*, 5, 50, 2022.

792 Zhang, Y., Zhao, T., Ning, G., Xu, X., Chen, Z., Jia, M., Sun, X., Shu, Z., Lu, Z., and Liu, J.: A unique  
793 mechanism of ozone surges jointly triggered by deep stratospheric intrusions and the Tibetan Plateau  
794 topographic forcing, *Geophysical Research Letters*, 52, e2024GL114207, 2025.

795 Zhang, Z., Jiang, Z., Zhou, T., and Geng, L.: Reconciling Modeled and Observed  $\Delta^{17}\text{O}(\text{NO}_3^-)$  in  
796 Beijing Winter Haze With Heterogeneous Chlorine Chemistry, *Journal of Geophysical Research:*  
797 *Atmospheres*, 129, e2023JD039740, <https://doi.org/10.1029/2023JD039740>, 2024.

798 Zhao, M., Huang, Z., Qiao, T., Zhang, Y., Xiu, G., and Yu, J.: Chemical characterization, the transport  
799 pathways and potential sources of  $\text{PM}_{2.5}$  in Shanghai: Seasonal variations, *Atmospheric Research*,  
800 158, 66-78, 2015.

801 Zong, Z., Tan, Y., Wang, X., Tian, C., Li, J., Fang, Y., Chen, Y., Cui, S., and Zhang, G.: Dual-modelling-  
802 based source apportionment of  $\text{NO}_x$  in five Chinese megacities: Providing the isotopic footprint  
803 from 2013 to 2014, *Environment International*, 137, 105592,  
804 <https://doi.org/10.1016/j.envint.2020.105592>, 2020.

805